

RESEARCH ARTICLE | JANUARY 31 2022

Simulating the dynamics of electronic observables via reduced-dimensionality generalized quantum master equations

Ellen Mulvihill ; Eitan Geva  



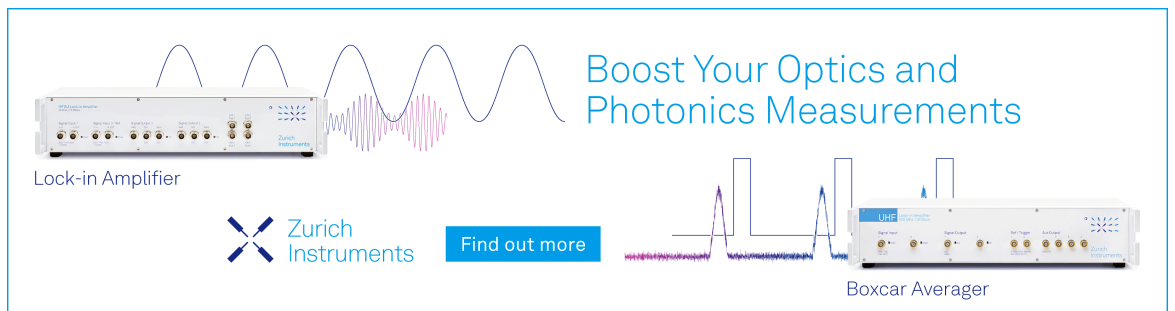
J. Chem. Phys. 156, 044119 (2022)

<https://doi.org/10.1063/5.0078040>

 CHORUS




CrossMark



Boost Your Optics and Photonics Measurements

Lock-in Amplifier

 Zurich Instruments

[Find out more](#)

Boxcar Averager

Simulating the dynamics of electronic observables via reduced-dimensionality generalized quantum master equations

Cite as: J. Chem. Phys. 156, 044119 (2022); doi: 10.1063/5.0078040

Submitted: 9 November 2021 • Accepted: 10 January 2022 •

Published Online: 31 January 2022



View Online



Export Citation



CrossMark

Ellen Mulvihill  and Eitan Geva^{a)} 

AFFILIATIONS

Department of Chemistry, University of Michigan, Ann Arbor, Michigan 48109, USA

^{a)} Author to whom correspondence should be addressed: eitan@umich.edu

ABSTRACT

We describe a general-purpose framework for formulating the dynamics of any subset of electronic reduced density matrix elements in terms of a formally exact generalized quantum master equation (GQME). Within this framework, the effect of coupling to the nuclear degrees of freedom, as well as to any projected-out electronic reduced density matrix elements, is captured by a memory kernel and an inhomogeneous term, whose dimensionalities are dictated by the number of electronic reduced density matrix elements included in the subset of interest. We show that the memory kernel and inhomogeneous term within such GQMEs can be calculated from projection-free inputs of the same dimensionality, which can be cast in terms of the corresponding subsets of overall system two-time correlation functions. The applicability and feasibility of such reduced-dimensionality GQMEs is demonstrated on the two-state spin-boson benchmark model. To this end, we compare and contrast the following four types of GQMEs: (1) a full density matrix GQME, (2) a single-population scalar GQME, (3) a populations-only GQME, and (4) a subset GQME for any combination of populations and coherences. Using a method based on the mapping Hamiltonian approach and linearized semiclassical approximation to calculate the projection-free inputs, we find that while single-population GQMEs and subset GQMEs containing only one population are less accurate, they can still produce reasonable results and that the accuracy of the results obtained via the populations-only GQME and a subset GQME containing both populations is comparable to that obtained via the full density matrix GQMEs.

Published under an exclusive license by AIP Publishing. <https://doi.org/10.1063/5.0078040>

I. INTRODUCTION

A variety of important chemical processes, ranging from photosynthesis to photovoltaics, involve multiple intricately interconnected electronic energy, charge, and coherence transfer pathways.^{1–12} A quantitative molecular-level understanding of the inherently quantum-mechanical dynamics underlying these pathways and their interplay with decoherence, which is key for function–structure relations as well as rational design principles in biologically and technologically relevant molecular systems, remains one of the most formidable challenges facing computational chemistry. The exponential scaling of the computational cost with system dimensionality makes quantum-mechanically exact simulations of the entire molecular system [i.e., electronic + nuclear degrees of freedom (DOF)] non-feasible in complex molecular systems, with the exception of a rather restrictive subclass of Hamiltonians

whose form makes such a quantum-mechanically exact simulation possible.^{13–19} Thus, general-purpose reduced-dimensionality approaches that focus on the dynamics of the electronic observables of interest are called for.

The generalized quantum master equation (GQME) formalism, which was introduced by Nakajima²⁰ and Zwanzig²¹ more than sixty years ago, provides a formal framework for developing such a general-purpose reduced-dimensionality approach that focuses on the dynamics of the electronic DOF of interest while keeping the information on the remaining DOF to the minimum necessary in order to capture their effect on the electronic DOF of interest. Within the GQME approach, the electronic DOF of interest are treated as a quantum open system whose dynamics is described by a formally exact equation of motion (the so-called GQME) derived by projecting out the remaining DOF. Within this equation of motion, or GQME, the effect of the projected-out DOF on the dynamics of

the electronic DOF of interest is formulated in terms of a *memory kernel* and an *inhomogeneous term*. The memory kernel and inhomogeneous term correspond to the minimum information about the projected-out DOF that is needed in order to fully capture their effect on the electronic DOF of interest.

A significant amount of effort over the last two decades has been directed at developing, testing, and applying computational methods for calculating the memory kernel within the GQME formalism for the case where the electronic observable of interest corresponds to the entire electronic reduced density matrix. These efforts were mostly based on the fact that the memory kernel can be calculated from projection-free inputs (PFIs), which can be obtained using either quantum-mechanically exact or approximate semiclassical and mixed quantum-classical input methods.^{22–41} It should be noted that the fact that the memory kernel is often temporally as well as dimensionally compact makes it possible to limit the use of such exact or approximate methods to relatively short times, where they are often more accurate and/or more cost-effective. Indeed, pursuing such an approach has often been observed to produce results that are more accurate than those obtained via direct application of the approximate method of choice at a reduced computational cost.

However, the focus on the entire reduced electronic density matrix as the observable of interest also made it challenging to scale up the approach with respect to the number of electronic states. More specifically, the fact that the memory kernel corresponds to an $N_e^2 \times N_e^2$ super-matrix in the case of a system with N_e electronic states has restricted the use of the methodology, in practice, to systems with a relatively small number of electronic states ($N_e \sim 10$).

One strategy for addressing this challenge, which was recently introduced by Pfalzgraff *et al.*, is based on developing algorithms that accelerate the convergence of the PFIs, when calculated via mixed quantum-classical methods such as the Ehrenfest method, by dynamically adjusting the number of classical-like trajectories allocated for calculating a given matrix element based on its importance for the relaxation process of interest.³⁷ Indeed, using such an approach, Pfalzgraff *et al.* were able to extend the range of applicability of the GQME approach to such systems as the light-harvesting complex II (LHCII), which has $N_e = 14$ electronic states.

In this paper, we explore an alternative approach for scaling up the GQME approach that is based on utilizing the flexibility offered by the GQME formalism with respect to the choice of projection operator. To this end, we use the fact that it is possible to derive a GQME for *any* subset of electronic reduced density matrix elements of one's choice, as well as practical procedures for calculating the corresponding memory kernel and inhomogeneous term from PFIs. Importantly, the dimensionalities of the memory kernel, inhomogeneous term, and PFIs are dictated by the number of electronic reduced density matrix elements included in the subset of interest, thereby potentially making it possible to reduce the computational cost associated with their calculation and extend the range of applicability of the GQME approach. It should be noted that a similar approach has been previously discussed in Refs. 42 and 33. In this paper, we expand on the discussion in those papers in several ways, including comparing different types of projection operators, calculating the inhomogeneous term, and using a different semiclassical method for calculating the PFIs.

The remainder of this paper is organized as follows: The objectives and scope of our approach are discussed in Sec. II. The GQME

formalism and its different possible implementations using different projection operators, including ones that give rise to reduced-dimensionality GQMEs, are described in Sec. III. The utility of various types of GQMEs is demonstrated on a benchmark spin-boson model with PFIs calculated via a mapping Hamiltonian linearized semiclassical (LSC) method in Sec. IV. Concluding remarks are provided in Sec. V. Various technical aspects and further analysis are provided in Appendices A and B. Additional graphs and data are included in the [supplementary material](#).

II. PRELIMINARY CONSIDERATIONS

In what follows, we focus on GQMEs designed for molecular systems with an overall Hamiltonian of the following commonly encountered form:

$$\hat{H} = \sum_{j=1}^{N_e} \hat{H}_j |j\rangle \langle j| + \sum_{\substack{j,k=1 \\ k \neq j}}^{N_e} \hat{V}_{jk} |j\rangle \langle k|. \quad (1)$$

Here, $\hat{H}_j = \hat{\mathbf{P}}^2/2 + V_j(\hat{\mathbf{R}})$ is the nuclear Hamiltonian when the system is in the diabatic electronic state $|j\rangle$, with the index j running over the N_e electronic states; $\{\hat{V}_{jk} | j \neq k\}$ are coupling terms between electronic states (which can be either nuclear operators or constants); and $\hat{\mathbf{R}} = (\hat{R}_1, \dots, \hat{R}_{N_n})$ and $\hat{\mathbf{P}} = (\hat{P}_1, \dots, \hat{P}_{N_n})$ are the mass-weighted position and momentum operators of the $N_n \gg 1$ nuclear DOF. Throughout this paper, boldfaced variables, e.g., \mathbf{A} , indicate vector quantities; a hat over a variable, e.g., \hat{B} , indicates an operator quantity; and calligraphic font, e.g., \mathcal{L} , indicates a superoperator.

We also assume that the initial state of the overall system is of the following single-product form:

$$\hat{\rho}(0) = \hat{\rho}_n(0) \otimes \hat{\sigma}(0). \quad (2)$$

Here, $\hat{\rho}_n(0) = \text{Tr}_e\{\hat{\rho}(0)\}$ and $\hat{\sigma}(0) = \text{Tr}_n\{\hat{\rho}(0)\}$ are the reduced density operators that describe the initial states of the nuclear DOF and electronic DOF, respectively, and $\text{Tr}_e\{\cdot\}$ and $\text{Tr}_n\{\cdot\}$ stand for partially tracing over the electronic Hilbert space and the nuclear Hilbert space, respectively.

Given the overall system Hamiltonian and initial state in Eqs. (1) and (2), respectively, the overall system state at a later time t is given by the density operator

$$\begin{aligned} \hat{\rho}(t) &= e^{-i\hat{H}t/\hbar} \hat{\rho}_n(0) \otimes \hat{\sigma}(0) e^{i\hat{H}t/\hbar} \\ &\equiv e^{-i\mathcal{L}t/\hbar} \hat{\rho}_n(0) \otimes \hat{\sigma}(0). \end{aligned} \quad (3)$$

Here, $\mathcal{L}(\cdot) = [\hat{H}, \cdot]$ is the Liouvillian superoperator, with \hat{H} being the overall Hamiltonian given in Eq. (1). The reduced electronic density operator at time t is given by

$$\hat{\sigma}(t) = \text{Tr}_n\{\hat{\rho}(t)\} = \sum_{j,k=1}^{N_e} \sigma_{jk}(t) |j\rangle \langle k|. \quad (4)$$

The electronic populations and coherences, whose time evolution underlies decoherence as well as energy, charge, and coherence transfer dynamics, are given by $\{\sigma_{jj}(t) = \langle j|\hat{\sigma}(t)|j\rangle\}$ and $\{\sigma_{jk}(t) = \langle j|\hat{\sigma}(t)|k\rangle | j \neq k\}$, respectively.

III. GENERALIZED QUANTUM MASTER EQUATIONS

The QGME formalism provides a general framework for deriving *exact* equations of motion for observables of interest while keeping the information on the projected-out DOF to the minimum necessary in order to account for their effect on the observables of interest. Within this formalism, the dynamics of the projected state, $\mathcal{P}\hat{\rho}(t)$, for any projection superoperator \mathcal{P} that satisfies idempotence ($\mathcal{P}^2 = \mathcal{P}$) is given by the Nakajima–Zwanzig equation,^{43–46}

$$\begin{aligned} \frac{d}{dt}\mathcal{P}\hat{\rho}(t) = & -\frac{i}{\hbar}\mathcal{P}\mathcal{L}\mathcal{P}\hat{\rho}(t) - \frac{1}{\hbar^2}\int_0^t d\tau\mathcal{P}\mathcal{L}e^{-i\mathcal{Q}\mathcal{L}\tau/\hbar}\mathcal{Q}\mathcal{L}\mathcal{P}\hat{\rho}(t-\tau) \\ & - \frac{i}{\hbar}\mathcal{P}\mathcal{L}e^{-i\mathcal{Q}\mathcal{L}t/\hbar}\mathcal{Q}\hat{\rho}(0). \end{aligned} \quad (5)$$

Here, $\mathcal{Q} = 1 - \mathcal{P}$ is the complimentary projection superoperator to \mathcal{P} (i.e., \mathcal{Q} projects onto what \mathcal{P} projects out). Importantly, there is a lot of flexibility when it comes to the choice of projection superoperator, \mathcal{P} , and thereby observables of interest. Each such choice would, in turn, give rise to a different equation of motion, or QGME, for the observable quantity of interest, as dictated by the choice of projection superoperator (see below).

Describing electronic dynamics for a system governed by the Hamiltonian in Eq. (1) within the QGME formalism is based on choosing electronic quantities as the observables of interest while projecting out the nuclear DOF as well as any remaining electronic DOF. However, this still leaves a lot of flexibility when it comes to the choice of the observables of interest. We will demonstrate this in the remainder of this section by considering different choices of electronic observables of interest and deriving the QGMEs that they give rise to.

A. A QGME for the full electronic density matrix

A popular choice for the electronic observable of interest is the full reduced electronic density operator $\hat{\sigma}(t)$ [see Eq. (4)], which can be obtained by projecting out the nuclear DOF. This can be done in multiple ways that lead to different forms of the QGME, and yet all those forms represent *exact* equations of motion for $\hat{\sigma}(t)$.⁴¹ For the sake of concreteness, we will proceed with the QGME of the form proposed in Ref. 38, which was based on the following choice of projection superoperator:

$$\mathcal{P}^{\text{full}}(\hat{A}) = \hat{\rho}_n(0) \otimes \text{Tr}_n\{\hat{A}\}. \quad (6)$$

Here, \hat{A} is an arbitrary overall system operator that the projection superoperator \mathcal{P} operates on. Substituting $\mathcal{P}^{\text{full}}$ into Eq. (5) and performing a partial trace over the nuclear Hilbert space (Tr_n) yield the following equation of motion, or QGME, for $\hat{\sigma}(t)$:³⁸

$$\frac{d}{dt}\hat{\sigma}(t) = -\frac{i}{\hbar}\langle\mathcal{L}\rangle_n^0\hat{\sigma}(t) - \int_0^t d\tau\mathcal{K}^{\text{full}}(\tau)\hat{\sigma}(t-\tau). \quad (7)$$

Within this QGME, the effect of the projected-out nuclear DOF on the dynamics of $\hat{\sigma}(t)$ is fully accounted for by the following two electronic superoperators:

- The projected Liouvillian,

$$\langle\mathcal{L}\rangle_n^0 \equiv \text{Tr}_n\{\hat{\rho}_n(0)\mathcal{L}\}, \quad (8)$$

which can be represented by a *time-independent* $N_e^2 \times N_e^2$ matrix, and

- the memory kernel,

$$\mathcal{K}^{\text{full}}(\tau) = \frac{1}{\hbar^2}\text{Tr}_n\left\{\mathcal{L}e^{-i\mathcal{Q}^{\text{full}}\mathcal{L}\tau/\hbar}\mathcal{Q}^{\text{full}}\mathcal{L}\hat{\rho}_n(0)\right\}, \quad (9)$$

which can be represented by a *time-dependent* $N_e^2 \times N_e^2$ matrix.

While calculating the matrix elements of $\langle\mathcal{L}\rangle_n^0$ is straightforward, this is not the case for the matrix elements of $\mathcal{K}^{\text{full}}(\tau)$. Significant effort over the last two decades has been directed at developing, testing, and applying various computational schemes for calculating $\mathcal{K}^{\text{full}}(\tau)$. Those schemes were all based on the fact that $\mathcal{K}^{\text{full}}(\tau)$ can be obtained from PFIs by solving integral Volterra equations, as was first shown in Refs. 22–25. The PFIs can be calculated using either quantum-mechanically exact or approximate semiclassical and mixed quantum-classical input methods.^{22–41} Additional studies advanced the understanding of the pros and cons of different implementations and expanded the range of applications of such QGMEs.^{26–41}

The simulation of electronic dynamics based on Eq. (7) involves three steps: (1) the calculation of the PFIs necessary for calculating the memory kernel, which correspond to overall system two-time correlation functions; (2) the calculation of the memory kernel, $\mathcal{K}^{\text{full}}(\tau)$, by numerically solving the corresponding Volterra equation using the PFIs calculated in the first step; and (3) the numerical solution of the QGME [Eq. (7)] using the memory kernel calculated in the second step to obtain the time evolution of the reduced electronic density matrix, $\hat{\sigma}(t)$.

While there is some variety in how steps (1)–(3) are implemented,⁴¹ the scaling of the computational cost associated with different implementations with increasing N_e is similar and the computational cost typically becomes prohibitively expensive for a relatively modest number of electronic states ($N_e \sim 10$).³⁷ For the sake of concreteness, we will demonstrate this scaling on the implementation based on the QGME in Eq. (7).^{38–41} Within this implementation, step (2) corresponds to solving the following Volterra equation for $\mathcal{K}^{\text{full}}(\tau)$:³⁸

$$\mathcal{K}^{\text{full}}(\tau) = i\check{\mathcal{F}}(\tau) - \frac{1}{\hbar}\mathcal{F}(\tau)\langle\mathcal{L}\rangle_n^0 + i\int_0^\tau d\tau'\mathcal{F}(\tau-\tau')\mathcal{K}^{\text{full}}(\tau'). \quad (10)$$

Here, $\mathcal{F}(\tau)$ and $\check{\mathcal{F}}(\tau)$ are the PFIs, which are given by

$$\begin{aligned} \mathcal{F}(\tau) &= \frac{1}{\hbar}\text{Tr}_n\left\{\mathcal{L}e^{-i\mathcal{L}\tau/\hbar}\hat{\rho}_n(0)\right\}, \\ \check{\mathcal{F}}(\tau) &= -\frac{i}{\hbar^2}\text{Tr}_n\left\{\mathcal{L}e^{-i\mathcal{L}\tau/\hbar}\mathcal{L}\hat{\rho}_n(0)\right\}. \end{aligned} \quad (11)$$

Thus, given the PFIs $\mathcal{F}(\tau)$ and $\check{\mathcal{F}}(\tau)$, Eq. (10) is solved numerically via an iterative algorithm³⁸ for the projection-dependent $\mathcal{K}^{\text{full}}(\tau)$.

Importantly, $\mathcal{F}(\tau)$ and $\check{\mathcal{F}}(\tau)$ are given in terms of $N_e^2 \times N_e^2$ matrices. A closer inspection reveals that the matrix elements of $\mathcal{F}(\tau)$, $\{\mathcal{F}_{jk,uv}(\tau)\}$, can be given in terms of overall system two-time correlation functions of the form³⁸

$$\text{Tr}\left\{\hat{\rho}_n(0)|u\rangle\langle v|e^{i\hat{\mathbf{R}}\tau/\hbar}\Gamma(\hat{\mathbf{R}})|b\rangle\langle a|e^{-i\hat{\mathbf{R}}\tau/\hbar}\right\}, \quad (12)$$

TABLE I. Types of QGMEs and their corresponding projection operators. This table gives the type of QGME in the first column, the projection operator that corresponds to that QGME acting on the overall density matrix, $\hat{\rho}$, in the middle column, and the results of the projection operator acting on a two-state system in the last column.

Type of QGME	Projection operator	Two-state system
Full electronic density matrix	Equation (6): $\mathcal{P}^{\text{full}}(\hat{\rho}) = \hat{\rho}_n(0) \otimes \text{Tr}_n\{\hat{\rho}\}$	$\mathcal{P}^{\text{full}} \begin{pmatrix} \hat{\rho}_{11} & \hat{\rho}_{12} \\ \hat{\rho}_{21} & \hat{\rho}_{22} \end{pmatrix} = \hat{\rho}_n(0) \otimes \begin{pmatrix} \sigma_{11} & \sigma_{12} \\ \sigma_{21} & \sigma_{22} \end{pmatrix}$
Single population	Equation (13): $\mathcal{P}^{jj}(\hat{\rho}) = \text{Tr}\{[j\rangle\langle j \otimes \hat{1}_n] \hat{\rho}\} \hat{\rho}_n(0) \otimes j\rangle\langle j $	$\mathcal{P}^{11} \begin{pmatrix} \hat{\rho}_{11} & \hat{\rho}_{12} \\ \hat{\rho}_{21} & \hat{\rho}_{22} \end{pmatrix} = \hat{\rho}_n(0) \otimes \begin{pmatrix} \sigma_{11} & 0 \\ 0 & 0 \end{pmatrix}$
Populations-only	Equation (21): $\mathcal{P}^{\text{POP}} = \sum_{j=1}^{N_e} \mathcal{P}^{jj}$	$\mathcal{P}^{\text{POP}} \begin{pmatrix} \hat{\rho}_{11} & \hat{\rho}_{12} \\ \hat{\rho}_{21} & \hat{\rho}_{22} \end{pmatrix} = \hat{\rho}_n(0) \otimes \begin{pmatrix} \sigma_{11} & 0 \\ 0 & \sigma_{22} \end{pmatrix}$

where the nuclear operator $\Gamma(\hat{\mathbf{R}})$ is either (i) $V_j(\hat{\mathbf{R}}) - V_k(\hat{\mathbf{R}})$ with $a = j$ and $b = k$, (ii) $V_{ja}(\hat{\mathbf{R}})$ with $a \neq j$ and $b = k$, or (iii) $V_{bk}(\hat{\mathbf{R}})$ with $a = j$ and $b \neq k$ (terms with $a \neq j$ and $b \neq k$ do not occur) and $V_j(\hat{\mathbf{R}})$ and $V_{jk}(\hat{\mathbf{R}})$ are as defined in Eq. (1). Thus, calculating $\mathcal{F}(\tau)$ in step (1) reduces to calculating those two-time correlation functions. $\tilde{\mathcal{F}}(\tau)$ can also be described by two-time correlation functions that differ from Eq. (12) only in the presence of an additional nuclear operator before or after $\hat{\rho}_n(0)$. Once $\mathcal{K}^{\text{full}}(\tau)$ has been obtained from $\mathcal{F}(\tau)$ and $\tilde{\mathcal{F}}(\tau)$ by numerically solving Eq. (10) via an iterative algorithm, it is substituted back into the QGME [Eq. (7)], which is solved numerically via a Runge–Kutta fourth-order (RK4) algorithm.⁴⁰

Within the QGME-based scheme outlined above, calculating the PFIs $\mathcal{F}(\tau)$ and $\tilde{\mathcal{F}}(\tau)$ calls for calculating their N_e^4 matrix elements. Calculating the two-time correlation functions underlying those matrix elements via mixed quantum-classical methods typically requires averaging over $\sim 10^5 - 10^7$ classical-like trajectories per each of the N_e^2 initial states.^{37–41} While each of the N_e^2 initial states can be run in parallel, this requires extensive computational resources. Additionally, the Volterra equation for the memory kernel [Eq. (10)] is usually solved via an iterative algorithm whose computational cost scales like $\sim N_e^6$.

One approach for reducing the cost of calculating the PFIs, which was recently proposed by Pfalzgraff *et al.* in Ref. 37, is based on accelerating convergence by dynamically adjusting the number of classical-like trajectories allocated for calculating a given matrix element based on its importance for the relaxation process of interest. In what follows, we explore an alternative approach^{33,42} for dimensionality reduction and potentially lowering the computational cost, which is based on starting out with *reduced-dimensionality QGMEs* for a subset of matrix elements of the reduced electronic density matrix, including *scalar QGMEs* where the quantity of interest as well as the projected Liouvillian and memory kernel correspond to scalar quantities (see Table I).

B. A scalar single-population QGME

In this subsection, we consider the case where the electronic observable of interest corresponds to the population of one particular electronic state, $\sigma_{jj}(t)$. It should be noted that a single-population QGME similar to that developed in this subsection was recently also considered by Ng *et al.*, who also derived a closed form expression for the corresponding memory kernel in the case of a purely electronic two-state system.⁴² In what follows, we go beyond that

by developing a general procedure for calculating the memory kernel and inhomogeneous term from PFIs and demonstrating it, with PFIs obtained via an approximate method, on a model system that involves nuclear as well as electronic DOF.

The equation of motion for $\sigma_{jj}(t)$, or *single-population QGME*, can be obtained by substituting the following projection superoperator into Eq. (5) ($\hat{1}_n$ is the nuclear identity operator):

$$\mathcal{P}^{jj}(\hat{A}) = \text{Tr}\{[|j\rangle\langle j| \otimes \hat{1}_n] \hat{A}\} \hat{\rho}_n(0) \otimes |j\rangle\langle j| \quad (13)$$

and tracing over both nuclear and electronic Hilbert spaces ($\text{Tr} = \text{Tr}_n \text{Tr}_e$). This results in the following *scalar* QGME for $\sigma_{jj}(t)$:

$$\frac{d}{dt} \sigma_{jj}(t) = - \int_0^t d\tau K^{jj}(\tau) \sigma_{jj}(t - \tau) + I^{jj}(t). \quad (14)$$

A comparison to Eq. (7) reveals that this QGME lacks a Liouvillian term, includes a memory kernel term where $K^{jj}(\tau)$ is the memory kernel, and also includes an additional so-called *inhomogeneous term*, $I^{jj}(t)$, which accounts for the effect of the initial state on $\sigma_{jj}(t)$. The memory kernel and inhomogeneous term are explicitly given by

$$K^{jj}(\tau) = \frac{1}{\hbar^2} \text{Tr}\{(|j\rangle\langle j| \otimes \hat{1}_n) \mathcal{L} e^{-i\mathcal{Q}^j \mathcal{L} \tau / \hbar} \mathcal{Q}^{jj} \mathcal{L} \hat{\rho}_n(0) \otimes |j\rangle\langle j|\}, \quad (15)$$

$$I^{jj}(t) = - \frac{i}{\hbar} \text{Tr}\{(|j\rangle\langle j| \otimes \hat{1}_n) \mathcal{L} e^{-i\mathcal{Q}^j \mathcal{L} t / \hbar} \times [\hat{\rho}(0) - \hat{\rho}_n(0) \otimes |j\rangle\langle j| \sigma_{jj}(0)]\}. \quad (16)$$

It should be noted that $K^{jj}(\tau)$ and $I^{jj}(t)$ are scalar quantities. This should be contrasted with $\mathcal{K}^{\text{full}}(\tau)$, which corresponds to an $N_e^2 \times N_e^2$ matrix. It should also be noted that $K^{jj}(\tau)$ is distinctly different from the corresponding (jj, jj) matrix elements of $\mathcal{K}^{\text{full}}(\tau)$ and that unlike the QGME for the full density matrix [Eq. (7)], the inhomogeneous term does not always vanish. For example, given that the initial state of the overall system is of the form $\hat{\rho}(0) = \hat{\rho}_n(0) \otimes |k\rangle\langle k|$, it can be shown that while $I_{jj}(t) = 0$ when $j = k$, $I_{jj}(t) \neq 0$ when $j \neq k$.

Importantly, despite the dramatic reduction in dimensionality compared to Eq. (7), Eq. (14) still corresponds to an *exact* equation of motion for $\sigma_{jj}(t)$. Thus, provided that $K^{jj}(\tau)$ and $I^{jj}(t)$ can be estimated accurately, Eq. (14) is guaranteed to yield the dynamics of $\sigma_{jj}(t)$ as accurately as the full electronic density matrix QGME [Eq. (7)] would.

TABLE II. PFIs for a two-state system. This table gives elements of $\mathcal{F}(\tau)$ that serve as PFIs in the case of the full electronic density matrix GQME in the first column, the elements of $F(\tau)$ that serve as PFIs in the case of the populations-only GQME in the second column, and elements of $F(\tau)$ that serve as PFIs in the case of the single-population scalar GQME in the third column. The elements are color-coded to show which elements are the same across the PFIs for the three types of GQMEs. In this example, the initial state of the system is $\hat{\rho} = \hat{\rho}_n(0) \otimes |1\rangle\langle 1|$ to show how the single-population scalar PFI $Z^{jj}(\tau)$ is equivalent to $-i\mathcal{F}_{jj,aa}(\tau)$ and $-i\mathcal{F}_{jj,aa}(\tau)$ from the full electronic density matrix PFIs and populations-only PFIs, respectively, when the initial state is in single-product form, i.e., $\hat{\rho}(0) = \hat{\rho}_n(0) \otimes |\alpha\rangle\langle\alpha|$. The elements of $\dot{\mathcal{F}}_{jj,kk}(\tau)$, $\dot{F}_{jj,kk}(\tau)$, and $\dot{F}^{jj}(\tau)$ follow the same pattern of equivalence as those of $\mathcal{F}_{jj,kk}(\tau)$, $F_{jj,kk}(\tau)$, and $F^{jj}(\tau)$.

Full electronic density matrix PFIs	Populations-only PFIs	Single-population scalar PFIs
$\begin{pmatrix} \mathcal{F}_{11,11}(\tau) & \mathcal{F}_{11,12}(\tau) & \mathcal{F}_{11,21}(\tau) & \mathcal{F}_{11,22}(\tau) \\ \mathcal{F}_{12,11}(\tau) & \mathcal{F}_{12,12}(\tau) & \mathcal{F}_{12,21}(\tau) & \mathcal{F}_{12,22}(\tau) \\ \mathcal{F}_{21,11}(\tau) & \mathcal{F}_{21,12}(\tau) & \mathcal{F}_{21,21}(\tau) & \mathcal{F}_{21,22}(\tau) \\ \mathcal{F}_{22,11}(\tau) & \mathcal{F}_{22,12}(\tau) & \mathcal{F}_{22,21}(\tau) & \mathcal{F}_{22,22}(\tau) \end{pmatrix}$	$\begin{pmatrix} F_{11,11}(\tau) & F_{11,22}(\tau) \\ F_{22,11}(\tau) & F_{22,22}(\tau) \end{pmatrix}$	$\begin{matrix} F^{11}(\tau) \\ F^{22}(\tau) \\ iZ^{22}(\tau) \end{matrix}$

Similar to $\mathcal{K}^{\text{full}}(\tau)$, $K^{jj}(\tau)$ can also be obtained from PFIs by solving the following Volterra equation [the derivation of Eq. (17) is provided in Appendix A]:

$$K^{jj}(\tau) = i\dot{F}^{jj}(\tau) + i \int_0^\tau d\tau' F^{jj}(\tau - \tau')K^{jj}(\tau'), \quad (17)$$

where the PFIs are given by

$$\begin{aligned} F^{jj}(\tau) &= \frac{1}{\hbar} \text{Tr}\left\{(|j\rangle\langle j| \otimes \hat{\mathbf{1}}_n) \mathcal{L}e^{-i\mathcal{L}\tau/\hbar} \hat{\rho}_n(0) \otimes |j\rangle\langle j|\right\}, \\ \dot{F}^{jj}(\tau) &= -\frac{i}{\hbar^2} \text{Tr}\left\{(|j\rangle\langle j| \otimes \hat{\mathbf{1}}_n) \mathcal{L}e^{-i\mathcal{L}\tau/\hbar} \mathcal{L} \hat{\rho}_n(0) \otimes |j\rangle\langle j|\right\}. \end{aligned} \quad (18)$$

Furthermore, $I^{jj}(\tau)$ can also be obtained from PFIs by solving another Volterra equation (see Appendix A),

$$I^{jj}(t) = Z^{jj}(t) + iF^{jj}(t)\sigma_{jj}(0) + i \int_0^t d\tau F^{jj}(t - \tau)I^{jj}(\tau), \quad (19)$$

where the PFI $F^{jj}(t)$ is as given in Eq. (18) and the PFI $Z^{jj}(t)$ is given by

$$Z^{jj}(t) = -\frac{i}{\hbar} \text{Tr}\left\{(|j\rangle\langle j| \otimes \hat{\mathbf{1}}_n) \mathcal{L}e^{-i\mathcal{L}t/\hbar} \hat{\rho}(0)\right\}. \quad (20)$$

Notably, the scalar PFIs $F^{jj}(\tau)$ and $\dot{F}^{jj}(\tau)$ correspond to the specific matrix elements $\mathcal{F}_{jj,jj}(\tau)$ and $\dot{\mathcal{F}}_{jj,jj}(\tau)$, respectively [both $\mathcal{F}(\tau)$ and $\dot{\mathcal{F}}(\tau)$ are given in Eq. (11)]. Furthermore, if the overall initial state is of the commonly encountered form $\hat{\rho}(0) = \hat{\rho}_n(0) \otimes |k\rangle\langle k|$, then $Z^{jj}(t)$ is equivalent to $-i\mathcal{F}_{jj,kk}(t)$. In other words, the PFIs needed for calculating $K^{jj}(\tau)$ and $I^{jj}(t)$ correspond to a subset of the matrix elements of the PFIs needed for calculating $\mathcal{K}^{\text{full}}(\tau)$ (see Table II).

C. A populations-only GQME

In this subsection, we consider the case where the electronic observables of interest correspond to the populations of all electronic states, $[\sigma_{11}(t), \sigma_{22}(t), \dots, \sigma_{N_e N_e}(t)]$. It should be noted that a populations-only GQME similar to that developed in this subsection was previously also studied by Montoya-Castillo and Reichman.³³ More specifically, the NIBA-type GQME in Ref. 33 is such a populations-only GQME. Montoya-Castillo and Reichman also

introduced a procedure for calculating the memory kernel of the populations-only GQME from PFIs, but it differs from the procedure in this section in two notable ways: (1) the Volterra equation for the memory kernel incorporates different PFIs than the ones in this section and (2) these PFIs were given in a form specific to the spin-boson Hamiltonian, while the PFIs in this section are generally applicable. Additionally, the populations-only GQME in Ref. 33 did not contain a procedure for the inhomogeneous term, should it be necessary.

The equation of motion for $[\sigma_{11}(t), \sigma_{22}(t), \dots, \sigma_{N_e N_e}(t)]$ can be obtained by substituting the following projection superoperator into Eq. (5):

$$\mathcal{P}^{\text{POP}} = \sum_{j=1}^{N_e} \mathcal{P}^{jj} \quad (21)$$

and tracing over the nuclear Hilbert space. This leads to the GQME

$$\begin{aligned} \sum_{j=1}^{N_e} |j\rangle\langle j| \frac{d}{dt} \sigma_{jj}(t) &= -\sum_{j,k=1}^{N_e} |j\rangle\langle j| \int_0^t d\tau K_{jj,kk}^{\text{POP}}(\tau) \sigma_{kk}(t - \tau) \\ &\quad + \sum_{j=1}^{N_e} |j\rangle\langle j| I_{jj}^{\text{POP}}(t), \end{aligned} \quad (22)$$

where the memory kernel matrix elements are given by

$$K_{jj,kk}^{\text{POP}}(\tau) = \frac{1}{\hbar^2} \text{Tr}\left\{(|j\rangle\langle j| \otimes \hat{\mathbf{1}}_n) \mathcal{L}e^{-i\mathcal{Q}^{\text{POP}}\tau/\hbar} \mathcal{Q}^{\text{POP}} \mathcal{L} \hat{\rho}_n(0) \otimes |k\rangle\langle k|\right\} \quad (23)$$

and the inhomogeneous term vector elements are given by

$$\begin{aligned} I_{jj}^{\text{POP}}(t) &= -\frac{i}{\hbar} \text{Tr}\left\{(|j\rangle\langle j| \otimes \hat{\mathbf{1}}_n) \mathcal{L}e^{-i\mathcal{Q}^{\text{POP}}t/\hbar} \right. \\ &\quad \left. \times \left[\hat{\rho}(0) - \sum_{k=1}^{N_e} \hat{\rho}_n(0) \otimes |k\rangle\langle k| \sigma_{kk}(0) \right] \right\}. \end{aligned} \quad (24)$$

The memory kernel and inhomogeneous term in this case correspond to an $N_e \times N_e$ matrix and an N_e -dimensional vector, respectively. This should be contrasted with the memory kernel in the case of the GQME for the full electronic reduced density matrix [Eq. (7)], where the memory kernel corresponds to an $N_e^2 \times N_e^2$

matrix (and the inhomogeneous term would have corresponded to an N_e^2 -dimensional vector if it did not vanish). It should be noted that $I_{jj}^{\text{POP}}(t) = 0$ when the initial electronic reduced density matrix is diagonal, $\sigma_{jk}(0) = \delta(j, k)\sigma_{jj}(0)$.

Here too, $\{K_{jj,kk}^{\text{POP}}(\tau)\}$ can be obtained from PFIs by solving the following set of N_e^2 coupled Volterra equations [the derivation of Eq. (25) is provided in Appendix A]:

$$K_{jj,kk}^{\text{POP}}(\tau) = i\dot{F}_{jj,kk}(\tau) + i\sum_{\lambda=1}^{N_e} \int_0^\tau d\tau' F_{jj,\lambda\lambda}(\tau - \tau') K_{\lambda\lambda,kk}^{\text{POP}}(\tau'), \quad (25)$$

where the PFIs are given by

$$F_{jj,kk}(\tau) = \frac{1}{\hbar} \text{Tr}\left\{(|j\rangle\langle j| \otimes \hat{1}_n) \mathcal{L}e^{-i\mathcal{L}\tau/\hbar} \hat{\rho}_n(0) \otimes |k\rangle\langle k|\right\}, \quad (26)$$

$$\dot{F}_{jj,kk}(\tau) = -\frac{i}{\hbar^2} \text{Tr}\left\{(|j\rangle\langle j| \otimes \hat{1}_n) \mathcal{L}e^{-i\mathcal{L}\tau/\hbar} \mathcal{L} \hat{\rho}_n(0) \otimes |k\rangle\langle k|\right\}.$$

It should be noted that the PFIs in this case correspond to a subset of the matrix elements of the $N_e^2 \times N_e^2$ matrices that serve as PFIs for obtaining $\mathcal{K}^{\text{full}}(\tau)$ [see Eq. (11)]. More specifically, the PFIs needed for calculating $\{K_{jj,kk}^{\text{POP}}(\tau)\}$ correspond to the N_e^2 (jj, kk) elements of the $N_e^2 \times N_e^2$ matrices that represent $\mathcal{F}(\tau)$ and $\dot{\mathcal{F}}(\tau)$ (see Table II).

The N_e vector elements of the inhomogeneous term $\{I_{11}^{\text{POP}}(t), \dots, I_{N_e, N_e}^{\text{POP}}(t)\}$ can also be obtained from PFIs by solving the following set of N_e coupled Volterra equations (see Appendix A):

$$I_{jj}^{\text{POP}}(t) = Z^{jj}(t) + i\sum_{k=1}^{N_e} F_{jj,kk}(t) \sigma_{kk}(0) + i\sum_{\lambda=1}^{N_e} \int_0^t d\tau F_{jj,\lambda\lambda}(t - \tau) I_{\lambda\lambda}^{\text{POP}}(\tau), \quad (27)$$

where $\{Z^{jj}(t)\}$ is as given in Eq. (20).

D. A subset GQME for any combination of populations and coherences

In this subsection, we consider the case where the electronic observables of interest correspond to a subset of the electronic reduced density matrix elements, $\{\sigma_{ab}(t)\}$. It should be noted that this GQME can be used to obtain the previous three GQMEs outlined in this section: the full GQME can be obtained by setting $\{ab\} = \{11, 12, \dots, 21, 22, \dots, N_e N_e\}$, the populations-only GQME can be obtained by setting $\{ab\} = \{11, 22, \dots, N_e N_e\}$, and the single-population scalar GQME can be obtained by setting $\{ab\} = \{jj\}$.

The equation of motion for $\{\sigma_{ab}(t)\}$ can be obtained by substituting the following projection superoperator into Eq. (5):

$$\mathcal{P}^{\text{sub}} \hat{A} = \sum_{jk \in \{ab\}} \mathcal{P}^{jk} \hat{A} = \sum_{jk \in \{ab\}} \text{Tr}\left\{(|k\rangle\langle j| \otimes \hat{1}_n) \hat{A}\right\} \hat{\rho}_n(0) \otimes |j\rangle\langle k| \quad (28)$$

and tracing over the nuclear Hilbert space. This leads to the GQME,

$$\sum_{jk \in \{ab\}} |j\rangle\langle k| \frac{d}{dt} \sigma_{jk}(t) = -\frac{i}{\hbar} \sum_{\substack{jk \in \{ab\} \\ lm \in \{ab\}}} |j\rangle\langle k| \langle \mathcal{L}_{jk,lm} \rangle_n^0 \sigma_{lm}(t) - \sum_{\substack{jk \in \{ab\} \\ lm \in \{ab\}}} |j\rangle\langle k| \int_0^t d\tau K_{jk,lm}^{\text{sub}}(\tau) \sigma_{lm}(t - \tau) + \sum_{jk \in \{ab\}} |j\rangle\langle k| I_{jk}^{\text{sub}}(t), \quad (29)$$

where the memory kernel matrix elements are given by

$$K_{jk,lm}^{\text{sub}}(\tau) = \frac{1}{\hbar^2} \text{Tr}\left\{(|k\rangle\langle j| \otimes \hat{1}_n) \mathcal{L}e^{-i\mathcal{Q}^{\text{sub}}\mathcal{L}\tau/\hbar} \times \mathcal{Q}^{\text{sub}} \mathcal{L} \hat{\rho}_n(0) \otimes |l\rangle\langle m|\right\} \quad (30)$$

and the inhomogeneous term vector elements are given by

$$I_{jk}^{\text{sub}}(t) = -\frac{i}{\hbar} \text{Tr}\left\{(|k\rangle\langle j| \otimes \hat{1}_n) \mathcal{L}e^{-i\mathcal{Q}^{\text{sub}}\mathcal{L}t/\hbar} \times \left[\hat{\rho}(0) - \sum_{lm \in \{ab\}} \hat{\rho}_n(0) \otimes |l\rangle\langle m| \sigma_{lm}(0)\right]\right\}. \quad (31)$$

Given N_{sub} equal to the number of elements in $\{\sigma_{ab}(t)\}$, the memory kernel and inhomogeneous term in this case correspond to an $N_{\text{sub}} \times N_{\text{sub}}$ matrix and an N_{sub} -dimensional vector, respectively.

The memory kernel $\{K_{jk,lm}^{\text{sub}}(\tau)\}$ can also be obtained from PFIs by solving the following set of N_{sub}^2 coupled Volterra equations [the derivation of Eq. (32) is provided in Appendix A]:

$$K_{jk,lm}^{\text{sub}}(\tau) = i\dot{F}_{jk,lm}(\tau) - \frac{1}{\hbar} \sum_{uv \in \{ab\}} F_{jk,uv}(\tau) \langle \mathcal{L}_{uv,lm} \rangle_n^0 + i \sum_{uv \in \{ab\}} \int_0^\tau d\tau' F_{jk,uv}(\tau - \tau') K_{uv,lm}^{\text{sub}}(\tau'), \quad (32)$$

where the PFIs are given by

$$F_{jk,lm}(\tau) = \frac{1}{\hbar} \text{Tr}\left\{(|k\rangle\langle j| \otimes \hat{1}_n) \mathcal{L}e^{-i\mathcal{L}\tau/\hbar} \hat{\rho}_n(0) \otimes |l\rangle\langle m|\right\}, \quad (33)$$

$$\dot{F}_{jk,lm}(\tau) = -\frac{i}{\hbar^2} \text{Tr}\left\{(|k\rangle\langle j| \otimes \hat{1}_n) \mathcal{L}e^{-i\mathcal{L}\tau/\hbar} \mathcal{L} \hat{\rho}_n(0) \otimes |l\rangle\langle m|\right\}.$$

It should be noted that the PFIs in this case correspond to a subset of the matrix elements of the $N_e^2 \times N_e^2$ matrices that serve as PFIs for obtaining $\mathcal{K}^{\text{full}}(\tau)$ [see Eq. (11)]. More specifically, the PFIs needed for calculating $\{K_{jk,lm}^{\text{sub}}(\tau)\}$ correspond to the N_{sub}^2 (jk, lm) elements of the $N_e^2 \times N_e^2$ matrices that represent $\mathcal{F}(\tau)$ and $\dot{\mathcal{F}}(\tau)$ (see Table II).

The N_{sub} vector elements of the inhomogeneous term $\{I_{jk}^{\text{sub}}(t)\}$ can also be obtained from PFIs by solving the following set of N_{sub} coupled Volterra equations (see Appendix A):

$$I_{jk}^{\text{sub}}(t) = Z^{jk}(t) + i \sum_{lm \in \{ab\}} F_{jk,lm}(t) \sigma_{lm}(0) + i \sum_{uv \in \{ab\}} \int_0^t d\tau F_{jk,uv}(t - \tau) I_{uv}^{\text{sub}}(\tau), \quad (34)$$

where $\{Z^{jk}(t)\}$ is given by

$$Z^{jk}(t) = -\frac{i}{\hbar} \text{Tr}\left\{\left(|k\rangle\langle j| \otimes \hat{1}_n\right) \mathcal{L}e^{-i\mathcal{L}t/\hbar} \hat{\rho}(0)\right\}. \quad (35)$$

If the overall initial state is of the commonly encountered form $\hat{\rho}(0) = \hat{\rho}_n(0) \otimes |\alpha\rangle\langle\alpha|$, then $Z^{jk}(t)$ is equivalent to $-i\mathcal{F}_{jk,\alpha\alpha}(t)$.

E. A GQME for any electronic observable

In this sub section, we outline a procedure to simulating the dynamics of *any* electronic observable in terms of GQMEs for electronic populations. To this end, consider a general electronic observable of interest that corresponds to the expectation value of the Hermitian electronic operator \hat{O}_e . Casting \hat{O}_e in terms of its eigen-representation, we obtain $\hat{O}_e = \sum_{j=1}^{N_e} \lambda_j |\lambda_j\rangle\langle\lambda_j|$, where $\hat{O}_e |\lambda_j\rangle = \lambda_j |\lambda_j\rangle$. Thus, the expectation value of \hat{O}_e is given by $\langle\hat{O}_e\rangle = \sum_{j=1}^{N_e} \lambda_j \langle\lambda_j|\hat{\sigma}|\lambda_j\rangle$, which means that it can be obtained from just the diagonal elements of the matrix that represents $\hat{\sigma}$ in terms of the eigen-basis of \hat{O}_e , $\{|\lambda_1\rangle, \dots, |\lambda_{N_e}\rangle\}$. Thus, a populations-only projection superoperator of the form of \mathcal{P}_{pop} for the electronic populations in terms of this eigen-basis would give rise to a GQME for the N_e -dimensional vector $\{\langle\lambda_1|\hat{\sigma}|\lambda_1\rangle, \dots, \langle\lambda_{N_e}|\hat{\sigma}|\lambda_{N_e}\rangle\}$ and thereby allow for the calculation of $\langle\hat{O}_e\rangle$.

To summarize, multiple types of GQMEs of various dimensionalities, which range from one-dimensional (scalar) to N_e^4 -dimensional, can be derived for any subset of electronic populations and coherences in terms of any electronic basis. Each of those GQMEs corresponds to the exact equation of motion for the subset of electronic observables it was written for, with the effect of the projected-out DOF accounted for by quantities such as the projected Liouvillian, memory kernel, and inhomogeneous term. The memory kernel and inhomogeneous term can be obtained from PFIs by solving the corresponding Volterra equation that can also be derived in each case. Finally, the PFIs for reduced-dimensionality GQMEs correspond to subsets of the PFIs for the full density matrix GQME.

IV. A DEMONSTRATIVE APPLICATION TO THE SPIN-BOSON MODEL

In this section, we demonstrate the applicability of the aforementioned four GQMEs [the full electronic density matrix GQME, Eq. (7); the scalar single-population GQME, Eq. (14); the populations-only GQME, Eq. (22); and the subset GQME, Eq. (29)] on a benchmark spin-boson model. To this end, we compare and contrast the population difference between the two electronic states as predicted by the four GQMEs with the PFIs calculated via a previously introduced method based on the mapping Hamiltonian approach and the LSC approximation that was labeled as LSCII.³⁹ It should be noted that LSCII has also been previously referred to as the linearized semiclassical initial value representation (LSC-IVR) method.⁴⁷ The reader is referred to Ref. 39 for a detailed discussion of the protocols used for calculating PFIs via LSCII.

A. Model

The spin-boson Hamiltonian has the form of Eq. (1) with $\{\hat{H}_j\}$ and $\{\hat{V}_{jk} \rightarrow V_{jk}\}$ given by

$$\begin{aligned} \hat{H}_1 &\equiv \hat{H}_D = \epsilon + \sum_{k=1}^{N_n} \frac{\hat{p}_k^2}{2} + \frac{1}{2} \omega_k^2 \hat{R}_k^2 - c_k \hat{R}_k, \\ \hat{H}_2 &\equiv \hat{H}_A = -\epsilon + \sum_{k=1}^{N_n} \frac{\hat{p}_k^2}{2} + \frac{1}{2} \omega_k^2 \hat{R}_k^2 + c_k \hat{R}_k, \end{aligned} \quad (36)$$

$$V_{12} \equiv V_{DA} = V_{21} \equiv V_{AD} = \Gamma.$$

Here, the two electronic states are designated as donor and acceptor ($|D\rangle$ and $|A\rangle$, respectively), 2ϵ is the shift in equilibrium energy between the donor (D) and acceptor (A) states, and Γ is a positive constant describing the electronic coupling between the donor and acceptor states. Since Γ is a constant, this system satisfies the Condon approximation.

The nuclear modes' frequencies and coupling coefficients, $\{\omega_k, c_k\}$, are sampled from an Ohmic spectral density with an exponential cutoff,

$$J(\omega) = \frac{\pi}{2} \sum_{k=1}^{N_n} \frac{c_k^2}{\omega_k} \delta(\omega - \omega_k) \xrightarrow{N_n \rightarrow \infty} \frac{\pi \hbar}{2} \xi \omega e^{-\omega/\omega_c}. \quad (37)$$

Here, ξ is the Kondo parameter and ω_c is the cutoff frequency. The reader is referred to Appendix C of Ref. 38 for a description of the procedure used to obtain a discrete set of N_n nuclear mode frequencies, $\{\omega_k\}$, and coupling coefficients, $\{c_k\}$, from the spectral density in Eq. (37).

The initial state is assumed to be of the form of Eq. (2), with $\hat{\sigma}(0) = |D\rangle\langle D|$ for all the GQMEs and the initial nuclear density operator given by

$$\hat{\rho}_n(0) = \frac{e^{-\beta(\hat{H}_D + \hat{H}_A)/2}}{\text{Tr}_n\{e^{-\beta(\hat{H}_D + \hat{H}_A)/2}\}}. \quad (38)$$

Calculations were carried out for five different sets of parameter values (see Table III). The model numbers for models 1, 2, 4, and 5 were chosen as such to match the model numbering of Refs. 38 and 39. Model 3 from Refs. 38 and 39 was not included due to the difficulty in converging its populations-only results. Models 1 and 2 correspond to systems with a bias between the donor and acceptor states ($\epsilon = 1.0$) and only differ with respect to the value of ω_c . Model 4 corresponds to a biased system with higher friction than models 1 and 2. Models 5 and 6 correspond to systems with zero bias between the donor and acceptor states ($\epsilon = 0.0$) that differ with respect to Γ , β , ξ , and ω_c . Model 6 was adopted from Ref. 30 in order to include a symmetric system for which exact results are available on a longer time scale compared to model 5. The results reported in this paper were obtained with a time step of $\Delta t = 0.005 \Gamma^{-1}$ and by averaging over $N_{\text{traj}} = 10^6$ trajectories for each initial state

TABLE III. Spin-boson model and simulation parameters.

Model No.	Model parameters					Numerical parameters				
	ϵ	Γ	β	ξ	ω_c	ω_{max}	N_n	Δt	N_{traj}	
1	1.0	1.0	5.0	0.1	1.0	5	400	0.005	10^6	
2	1.0	1.0	5.0	0.1	2.0	10	400	0.005	10^6	
4	1.0	1.0	5.0	0.4	2.0	10	400	0.005	10^6	
5	0.0	0.333	3.0	0.1	1.0	5	400	0.005	10^6	
6	0.0	1.0	5.0	0.2	2.5	12	400	0.005	10^6	

and model. Quantum-mechanically exact results were adopted from Ref. 34 for models 1–4, from Ref. 48 for model 5, and from Ref. 30 for model 6.

B. Results

Shown in Figs. 1 and 2 are the matrix elements of $\mathcal{F}(\tau)$ and $\dot{\mathcal{F}}(\tau)$, respectively [see Eq. (11)], for model 1 (see Table III), as obtained using LSCII as the input method. These matrix elements can be used for the PFIs of the reduced-dimensionality GQMEs, as discussed and demonstrated in Sec. III. Graphs with the matrix elements of the PFIs for the other four realizations of the spin-boson benchmark model described in Table III are included in the [supplementary material](#).

In Fig. 3, the real part of the matrix elements of the nine different memory kernels for model 1 (see Table III) is shown. While the grid has 16 graphs in it, only the full density matrix GQME memory kernel has elements in all 16 graphs. The other GQMEs, being of reduced dimensionality, have less memory kernel elements. Graphs with the imaginary part for model 1 along with the results for the other four realizations of the spin-boson benchmark model described in Table III are included in the [supplementary material](#). Shown in Fig. 4 is the single-population scalar inhomogeneous term $I^{11}(t)$ [see Eq. (16)] for model 1 (see Table III). Graphs with the inhomogeneous terms for the other four models in Table III are included in the [supplementary material](#).

In Figs. 5–9, we compare the time evolution of the electronic population difference, $\sigma_z(t) = \sigma_{DD}(t) - \sigma_{AA}(t)$, obtained based on single-population, populations-only, subset, and full density matrix GQMEs [Eqs. (14), (22), (29), and (7), respectively]. The results shown were obtained for the five realizations of the spin-boson benchmark model described in Table III using LSCII as the input method.³⁹ For each of the GQMEs, the values of $\sigma_{DD}(t)$ and $\sigma_{AA}(t)$ were calculated and then $\sigma_z(t)$ was obtained via $\sigma_z(t) = \sigma_{DD}(t) - \sigma_{AA}(t)$ [as opposed to obtaining $\sigma_{AA}(t)$ from $\sigma_{DD}(t)$, or vice versa, by using $\sigma_{DD}(t) + \sigma_{AA}(t) = 1$].

A close inspection of Figs. 5–9 reveals the following trends:

- Restricting the use of LSCII to calculating the PFIs yields more accurate results than the direct application of LSCII. This is particularly clear for models 1, 2, 4, and 6 (less so for model 5 for which exact results are available on a relatively short range). This observation is consistent with similar observations made previously in the context of the full density matrix GQME.³⁹ The results in Figs. 5–9 demonstrate that this is also the case for the single-population, populations-only, and subset GQMEs.
- From the GQMEs explored in this paper, the full density matrix GQME, the populations-only GQME, and the subset GQME with $\{ab\} = \{00, 01, 11\}$ yield the most consistently accurate results, while the combination of the single-population GQMEs, the combination of the subset

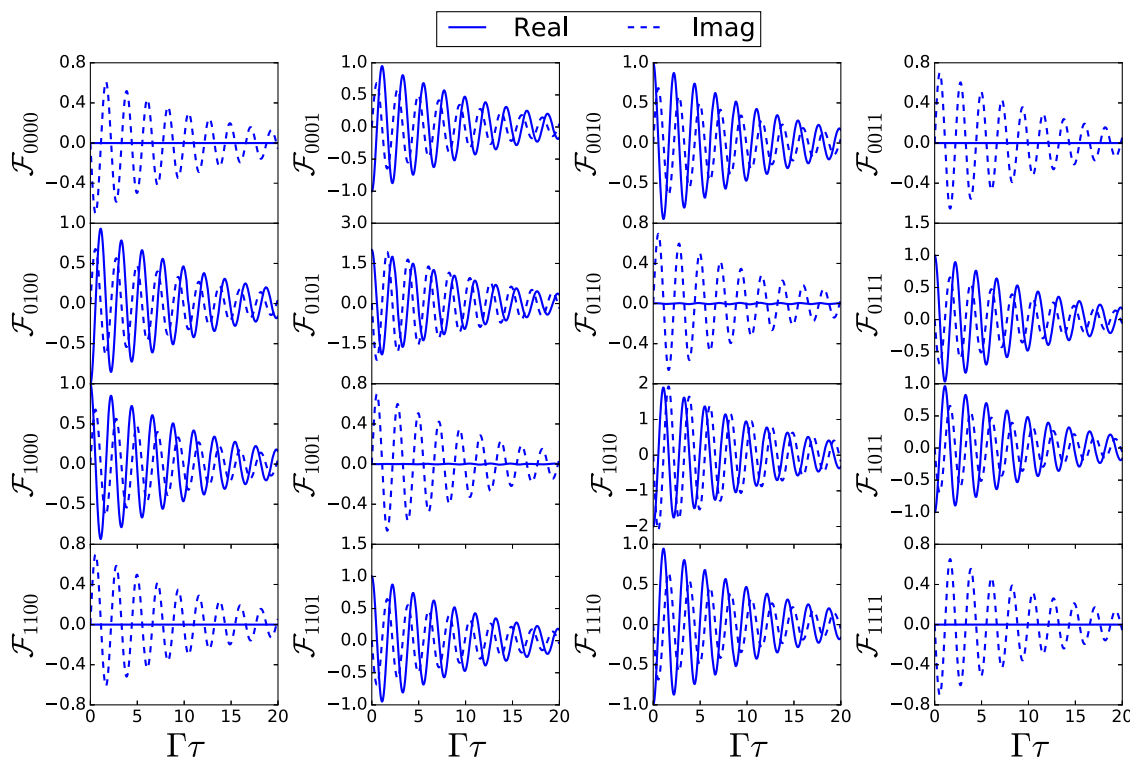


FIG. 1. Shown are the matrix elements of the PFI $\mathcal{F}(\tau)$, given in Eq. (11), for model 1 in Table III obtained with LSCII. The real part of each element is depicted by a solid line and the imaginary part is depicted by a dashed line. These matrix elements can be used for the PFIs of the reduced-dimensionality GQMEs as well. Graphs for the other four models in Table III are included in the [supplementary material](#).

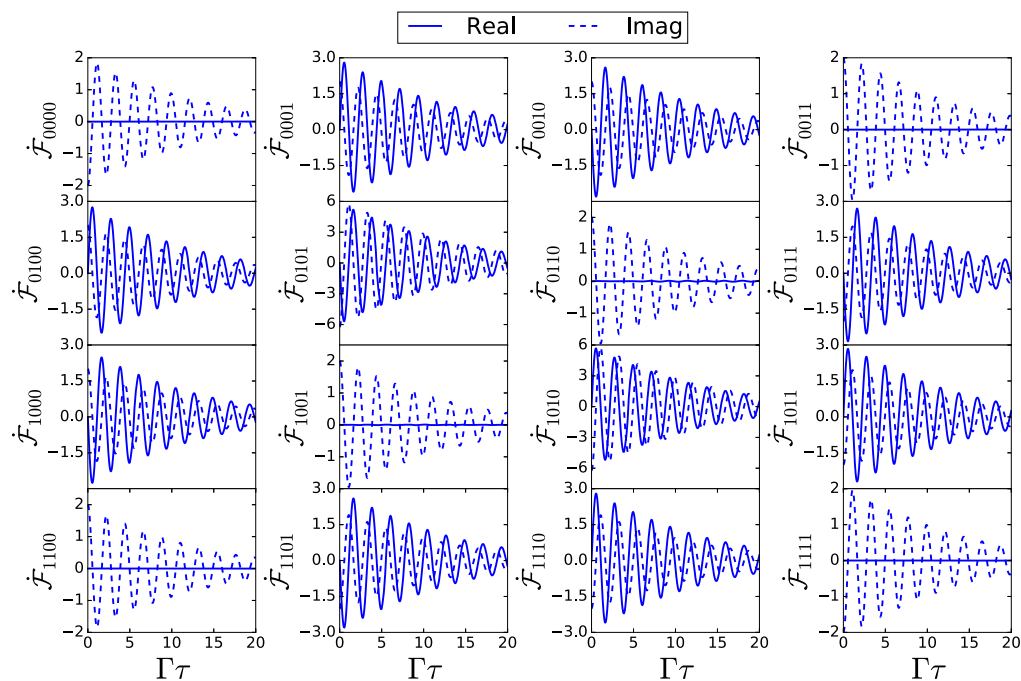


FIG. 2. Shown are the matrix elements of the PFI $\mathcal{F}(\tau)$, given in Eq. (11), for model 1 in Table III obtained with LSCII. The real part of each element is depicted by a solid line and the imaginary part is depicted by a dashed line. These matrix elements can be used for the PFIs of the reduced-dimensionality QMEs as well. Graphs for the other four models in Table III are included in the supplementary material.

GQMEs with $\{ab\} = \{00, 01\}$ and $\{ab\} = \{10, 11\}$, and the combination of the subset GQMEs with $\{ab\} = \{00, 01, 10\}$ and $\{ab\} = \{01, 10, 11\}$ are less accurate.

These differences in accuracy are likely due to the fact that projecting out the electronic populations and/or coherences causes the effect of those projected-out electronic matrix elements on the matrix elements of interest to be treated more approximately and could therefore lead to discrepancies when the approximate method used is less accurate. Indeed, the difference in accuracy is made more significant by making the model more quantum. Both trends are particularly clear in the case of models 2 and 4, where the relatively high cutoff frequency, relatively low temperature, and the non-zero energy bias between the donor and acceptor states conspire to make these the most challenging cases for quasiclassical approximate methods such as LSCII (see Figs. 6 and 7). However, it should be noted that the accuracy of the results obtained via the populations-only GQME and the subset GQME with $\{ab\} = \{00, 01, 11\}$ is still comparable to that obtained via the full density matrix GQME. This suggests that the coherences have a relatively small effect on the populations so that projecting them out and treating their effect in an approximate manner have a relatively small effect on the accuracy. This is less so when one also projects out the population of one of the states, as in the case of the single-population GQME and the subset GQMEs with $\{ab\} = \{00, 01\}$, $\{10, 11\}$, $\{00, 01, 10\}$, and $\{01, 10, 11\}$. The difference in the effect of projecting-out a population vs.

a coherence is not entirely surprising, as at least in Redfield theory, dephasing is affected by population relaxation, but population relaxations are not affected by dephasing. This can be traced back to the fact that inelastic interactions can change both phase and energy, while elastic collisions can only change the phase (so-called pure dephasing). Furthermore, within the secular approximation, the populations and coherences are decoupled within Redfield theory. In light of this, it looks sensible to hypothesize that the coupling between populations is expected to be stronger more generally so that projecting one of them out and treating it approximately would have a bigger effect on the accuracy (see Appendix B for a more detailed discussion on the origin and nature of those inaccuracies). However the results for models 1, 5, and 6 also suggest that single-population GQMEs and subsets without a population can still produce reasonably accurate results when the model is not overly quantum.

The results in Figs. 5–9 are encouraging since they suggest that reduced-dimensionality GQMEs can still produce reasonably accurate results.

C. Computational cost analysis

In this section, we examine the scaling of the computational cost of the GQME-based approach with respect to the dimensionality of the electronic observable of interest. To this end, we

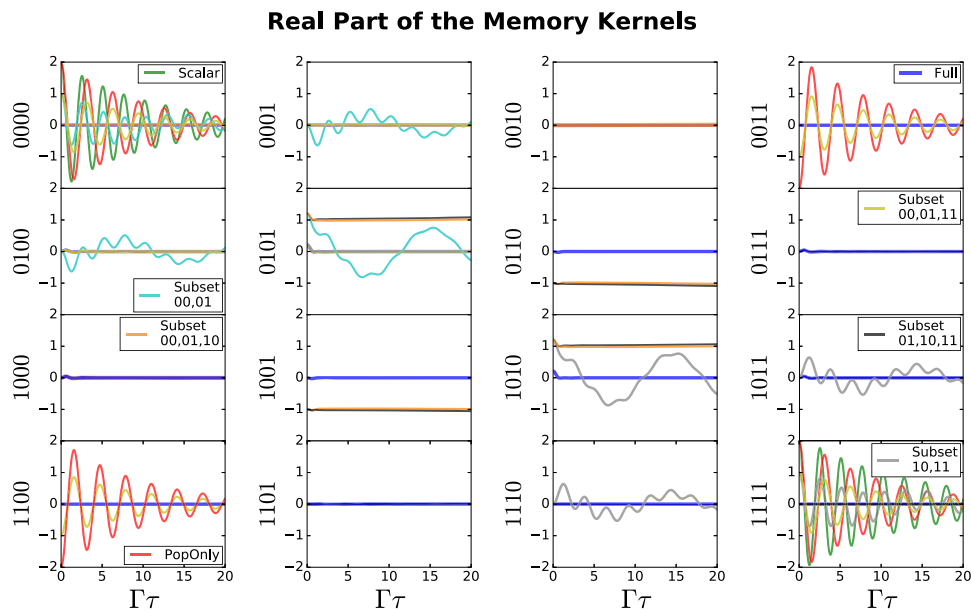


FIG. 3. Shown are the real part of the matrix elements of the memory kernels for model 1 in Table III obtained with LSCII-based PFIs. Depicted are the matrix elements of nine different memory kernels: (1) the memory kernel of the full GQME $K^{\text{full}}(\tau)$, given in Eq. (9), which is depicted with blue lines and has all 16 elements in the graphs above; (2) the memory kernel of a subset GQME $K^{\text{sub}}(\tau)$, given in Eq. (30), with $\{ab\} = \{00, 01, 11\}$, which is depicted with yellow lines and has nine elements: $\{0000, 0001, 0011, 0100, 0101, 0111, 1100, 1101, 1111\}$; (3) the memory kernel of a subset GQME $K^{\text{sub}}(\tau)$, with $\{ab\} = \{00, 01, 10\}$, which is depicted with orange lines and has nine elements: $\{0000, 0001, 0010, 0100, 0101, 0110, 1000, 1001, 1010\}$; (4) the memory kernel of a subset GQME $K^{\text{sub}}(\tau)$, with $\{ab\} = \{01, 10, 11\}$, which is depicted with black lines and has nine elements: $\{0101, 0110, 0111, 1001, 1010, 1011, 1101, 1110, 1111\}$; (5) the memory kernel of a subset GQME $K^{\text{sub}}(\tau)$, with $\{ab\} = \{00, 01\}$, which is depicted with cyan lines and has four elements: $\{0000, 0001, 0100, 0101\}$; (6) the memory kernel of a subset GQME $K^{\text{sub}}(\tau)$, with $\{ab\} = \{10, 11\}$, which is depicted with light gray lines and has four elements: $\{1010, 1011, 1110, 1111\}$; (7) the memory kernel of the populations-only GQME $K^{\text{pop}}(\tau)$, given in Eq. (23), which is depicted with red lines and has four elements: $\{0000, 0011, 1100, 1111\}$; and (8) and (9) the single-element memory kernels of the scalar single-population GQMEs $K^{00}(\tau)$ and $K^{11}(\tau)$, given in Eq. (15), which are depicted with green lines in the 0000 and 1111 elements, respectively. Graphs with the imaginary part for model 1 along with the results for the other four models are included in the supplementary material.

consider the scaling of the multiple computational components that the GQME-approach consists of: (1) the number of quasiclassical trajectories averaged over in order to obtain the PFIs, (2) the number of time steps per trajectory, (3) the number of initial electronic states that one needs to account for when calculating the PFIs, (4) the time of each iteration in the iterative Volterra algorithms for the memory kernel and inhomogeneous term, (5) the number of iterations required for the iterative Volterra algorithms to converge, (6) the necessity of the inhomogeneous term, and (7) the length of the memory time.

We look at each of these factors in more detail:

- (1) and (2): In general, the number of trajectories and time steps per trajectory needed for convergence of the electronic population difference with LSCII-based PFIs is similar for all the GQMEs used to obtain the results in this paper. To show this, included in the supplementary material are results obtained for ten sets of numerical parameters for each of the five models in this paper for each of the GQMEs used. Thus, the scaling of the computational cost with respect to time step and number of trajectories appears to be insensitive to the dimensionality of the electronic observable of interest.
- (3): When considering the number of initial states that one needs to account for when calculating the PFIs, it is

important to note that the matrix elements of $\hat{\mathcal{F}}(\tau)$ have the following form:

$$\begin{aligned} \hat{\mathcal{F}}_{abcd}(\tau) = & -\frac{i}{\hbar^2} \left[\text{Tr} \left\{ (\hat{H}_c \hat{\rho}_n(0) - \hat{\rho}_n(0) \hat{H}_d) |c\rangle \langle d| \hat{Y}(\tau) \right\} \right. \\ & + \sum_{\substack{j=1 \\ j \neq c}}^{N_e} \text{Tr} \left\{ \hat{V}_{jc} \hat{\rho}_n(0) |j\rangle \langle d| \hat{Y}(\tau) \right\} \\ & \left. - \sum_{\substack{k=1 \\ k \neq d}}^{N_e} \text{Tr} \left\{ \hat{\rho}_n(0) \hat{V}_{dk} |c\rangle \langle k| \hat{Y}(\tau) \right\} \right], \end{aligned}$$

where

$$\begin{aligned} \hat{Y}(\tau) = & e^{i\hat{H}\tau/\hbar} \left[(\hat{H}_a - \hat{H}_b) |b\rangle \langle a| + \sum_{\substack{l=1 \\ l \neq a}}^{N_e} \hat{V}_{al} |b\rangle \langle l| \right. \\ & \left. - \sum_{\substack{m=1 \\ m \neq b}}^{N_e} \hat{V}_{mb} |m\rangle \langle a| \right] e^{-i\hat{H}\tau/\hbar}. \end{aligned}$$

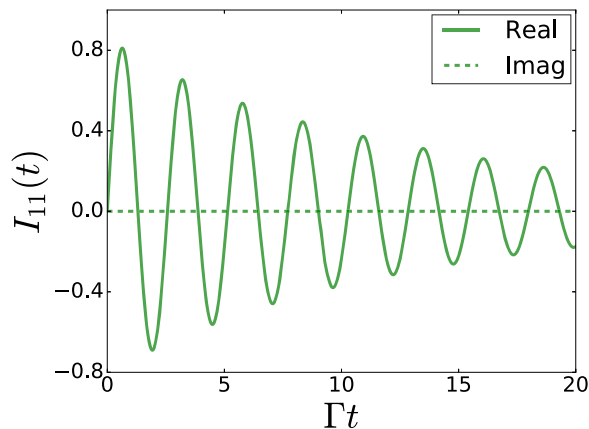


FIG. 4. Shown is the scalar single-population inhomogeneous term $I_{11}(t)$, given in Eq. (16), for model 1, obtained with LSCII-based PFIs. The real part is depicted with a solid green line and the imaginary part with a dashed green line. Graphs for the inhomogeneous terms of the other four models are included in the [supplementary material](#).

Thus, calculating the PFI $\hat{\mathcal{F}}_{abcd}(\tau)$ calls for the initial states $|c\rangle\langle d|$; $\{|j\rangle\langle d|\}$ for $j = 1, \dots, N_e$ with the condition that $j \neq c$; and $\{|c\rangle\langle k|\}$ for $k = 1, \dots, N_e$ with the condition that $k \neq d$. This means that the reduced-dimensionality GQMEs have less of an advantage when it comes to the number of initial states needed to be accounted for when calculating the

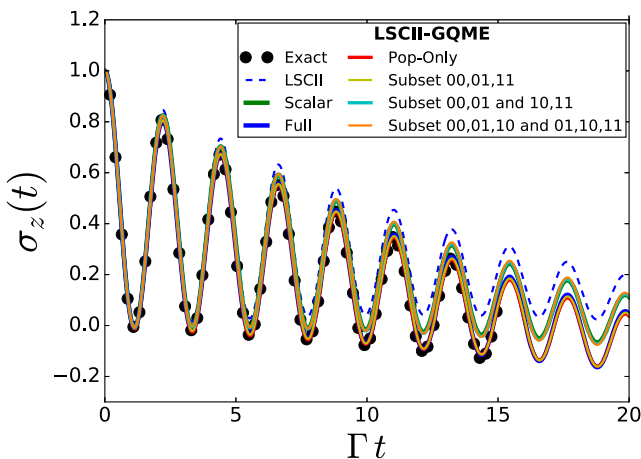


FIG. 5. Electronic population difference, $\sigma_z(t) = \sigma_{DD}(t) - \sigma_{AA}(t)$, as a function of time for model 1 in Table III. Shown are exact results (black circles) and results obtained based on the following: direct application of LSCII (dashed blue line); a combination of the two single-population scalar GQMEs of the form of Eq. (14) for $\sigma_{DD}(t)$ and $\sigma_{AA}(t)$ with LSCII-based PFIs (solid green line); a populations-only GQME of the form of Eq. (22) with LSCII-based PFIs (solid red line); a subset GQME of the form of Eq. (29) with $\{ab\} = \{00, 01, 11\}$ with LSCII-based PFIs (solid yellow line); a combination of two subset GQMEs with $\{ab\} = \{00, 01\}$ and $\{ab\} = \{10, 11\}$ with LSCII-based PFIs (solid cyan line); a combination of two subset GQMEs with $\{ab\} = \{00, 01, 10\}$ and $\{ab\} = \{01, 10, 11\}$ with LSCII-based PFIs (solid orange line); and the full density matrix GQME of the form of Eq. (7) with LSCII-based PFIs (solid blue line).

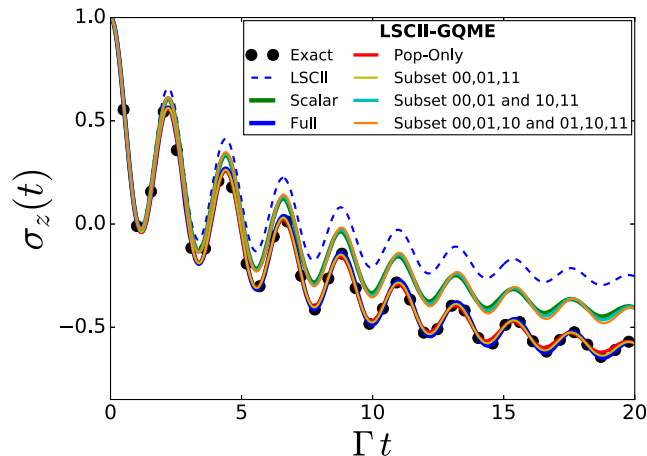


FIG. 6. Electronic population difference, $\sigma_z(t) = \sigma_{DD}(t) - \sigma_{AA}(t)$, as a function of time for model 2 in Table III. Shown are exact results (black circles) and results obtained based on the following: the direct application of LSCII (dashed blue line); a combination of the two single-population scalar GQMEs of the form of Eq. (14) for $\sigma_{DD}(t)$ and $\sigma_{AA}(t)$ with LSCII-based PFIs (solid green line); a populations-only GQME of the form of Eq. (22) with LSCII-based PFIs (solid red line); a subset GQME of the form of Eq. (29) with $\{ab\} = \{00, 01, 11\}$ with LSCII-based PFIs (solid yellow line); a combination of two subset GQMEs with $\{ab\} = \{00, 01\}$ and $\{ab\} = \{10, 11\}$ with LSCII-based PFIs (solid cyan line); a combination of two subset GQMEs with $\{ab\} = \{00, 01, 10\}$ and $\{ab\} = \{01, 10, 11\}$ with LSCII-based PFIs (solid orange line); and the full density matrix GQME of the form of Eq. (7) with LSCII-based PFIs (solid blue line).

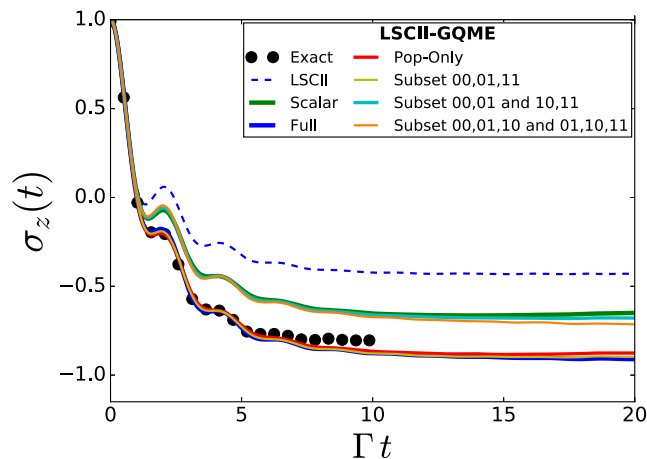


FIG. 7. Electronic population difference, $\sigma_z(t) = \sigma_{DD}(t) - \sigma_{AA}(t)$, as a function of time for model 4 in Table III. Shown are exact results (black circles) and results obtained based on the following: the direct application of LSCII (dashed blue line); a combination of the two single-population scalar GQMEs of the form of Eq. (14) for $\sigma_{DD}(t)$ and $\sigma_{AA}(t)$ with LSCII-based PFIs (solid green line); a populations-only GQME of the form of Eq. (22) with LSCII-based PFIs (solid red line); a subset GQME of the form of Eq. (29) with $\{ab\} = \{00, 01, 11\}$ with LSCII-based PFIs (solid yellow line); a combination of two subset GQMEs with $\{ab\} = \{00, 01\}$ and $\{ab\} = \{10, 11\}$ with LSCII-based PFIs (solid cyan line); a combination of two subset GQMEs with $\{ab\} = \{00, 01, 10\}$ and $\{ab\} = \{01, 10, 11\}$ with LSCII-based PFIs (solid orange line); and the full density matrix GQME of the form of Eq. (7) with LSCII-based PFIs (solid blue line).

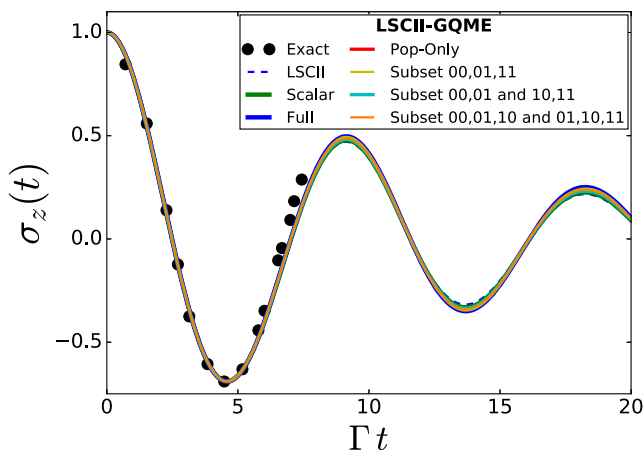


FIG. 8. Electronic population difference, $\sigma_z(t) = \sigma_{DD}(t) - \sigma_{AA}(t)$, as a function of time for model 5 in Table III. Shown are exact results (black circles) and results obtained based on the following: the direct application of LSCII (dashed blue line); a combination of the two single-population scalar GQMEs of the form of Eq. (14) for $\sigma_{DD}(t)$ and $\sigma_{AA}(t)$ with LSCII-based PFIs (solid green line); a populations-only GQME of the form of Eq. (22) with LSCII-based PFIs (solid red line); a subset GQME of the form of Eq. (29) with $\{ab\} = \{00, 01, 11\}$ with LSCII-based PFIs (solid yellow line); a combination of two subset GQMEs with $\{ab\} = \{00, 01\}$ and $\{ab\} = \{10, 11\}$ with LSCII-based PFIs (solid cyan line); a combination of two subset GQMEs with $\{ab\} = \{00, 01, 10\}$ and $\{ab\} = \{01, 10, 11\}$ with LSCII-based PFIs (solid orange line); and the full density matrix GQME of the form of Eq. (7) with LSCII-based PFIs (solid blue line).

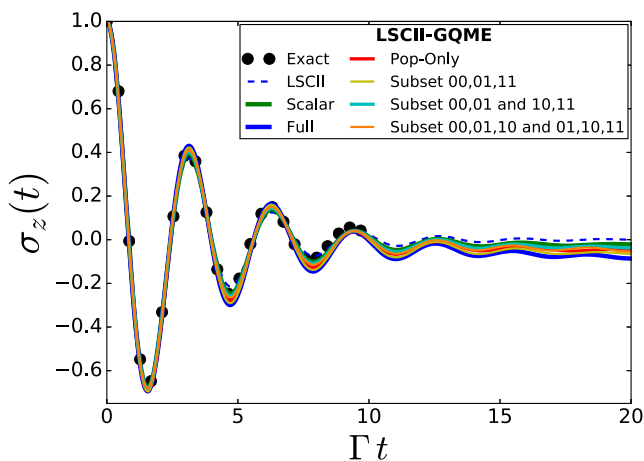


FIG. 9. Electronic population difference, $\sigma_z(t) = \sigma_{DD}(t) - \sigma_{AA}(t)$, as a function of time for model 6 in Table III. Shown are exact results (black circles) and results obtained based on the following: the direct application of LSCII (dashed blue line); a combination of the two single-population scalar GQMEs of the form of Eq. (14) for $\sigma_{DD}(t)$ and $\sigma_{AA}(t)$ with LSCII-based PFIs (solid green line); a populations-only GQME of the form of Eq. (22) with LSCII-based PFIs (solid red line); a subset GQME of the form of Eq. (29) with $\{ab\} = \{00, 01, 11\}$ with LSCII-based PFIs (solid yellow line); a combination of two subset GQMEs with $\{ab\} = \{00, 01\}$ and $\{ab\} = \{10, 11\}$ with LSCII-based PFIs (solid cyan line); a combination of two subset GQMEs with $\{ab\} = \{00, 01, 10\}$ and $\{ab\} = \{01, 10, 11\}$ with LSCII-based PFIs (solid orange line); and the full density matrix GQME of the form of Eq. (7) with LSCII-based PFIs (solid blue line).

PFIs than one may expect based on just the dimensionality. For example, three initial states are needed in the case of a scalar single-population GQME for a two-state model, compared to the four initial states needed for full density matrix GQME.

- (4): The computational complexity of each iteration in the Volterra algorithm for the memory kernel is expected to be $O(N_{\text{mat}}^3)$ and was found empirically to be $\sim 1.25 N_{\text{mat}}^3$ (based on the data included in the excel file in the [supplementary material](#)), where N_{mat} is the number of matrix elements in a row of the memory kernel super-matrix (e.g., $N_{\text{mat}} = N_e^2$ for the full GQME, $N_{\text{mat}} = N_e$ for the populations-only GQME, and $N_{\text{mat}} = 1$ for the single-population scalar GQME). It should be noted that using a non-iterative Volterra algorithm, as was done in Ref. 37, is expected to give rise to a similar computational complexity as a single iteration. Finally, we note that the computational complexity of each iteration in the Volterra algorithm for the inhomogeneous term is $O(N_{\text{mat}}^2)$.
- (5): The number of iterations required for the iterative Volterra algorithm for the memory kernel to converge is rather sensitive to the dimensionality of the electronic observable of interest. More specifically, for the spin-boson model, while 2–3 iterations were required for calculating the scalar single-population memory kernels and 2–4 iterations were needed in the case of the populations-only memory kernel for all the models and sets of parameters, 5–10 iterations were required in cases of higher dimensionality. The number of iterations required for the iterative Volterra algorithm for the inhomogeneous term was observed to follow a similar trend. While we do not know before running the Volterra algorithm how many iterations it will take and do not expect it to be the same number across different systems, this trend with respect to dimensionality that was observed for the spin-boson model could hold across systems. Further study is needed to confirm or reject this hypothesis.
- (6): The inhomogeneous term was only required for the scalar single-population GQME for $\sigma_{11}(t)$, and the subset GQMEs with subsets $\{ab\} = \{10, 11\}$ and $\{ab\} = \{01, 10, 11\}$ and would be required for any subset that did not contain the initial electronic state. Given the scaling of the Volterra algorithm for the inhomogeneous term and the observation that it is necessary to include all populations involved in the electronic dynamics to obtain the best improvement in accuracy with any subset GQME, it can be concluded that subsets requiring the calculation of the inhomogeneous term are less favorable.
- (7): The converged memory time for each of the models and GQME types was found using an algorithm similar to that from Appendix D of Ref. 39, although it checks all elements of the reduced electronic density matrix rather than just the electronic population difference, $\sigma_z(t)$. The full description of the convergence algorithm used for this paper is provided in the [supplementary material](#). The basic premise of the algorithm is to first calculate the dynamics at the highest possible memory time, $t_{\text{mem, max}}$, based on the maximum time of the PFI dynamics and then walk backward in memory time to find the shortest memory time that keeps

each element and time step of the electronic density matrix within a convergence parameter of the same element and time step of the dynamics with the highest possible memory time. For the models studied in this paper, the highest possible memory time was $t_{\text{mem, max}} = 20 \Gamma^{-1}$ and the converged memory time for each model and GQME type is given in the excel file within the [supplementary material](#). The full GQME typically corresponds to the shortest memory time, while the reduced-dimensionality GQMEs required significantly longer memory times. While the RK4 algorithm is expected to have computational complexity $O(t_{\text{mem}})$ and was found empirically to scale sublinearly with respect to the memory time, t_{mem} , the cost of a single iteration of the Volterra algorithm for the memory kernel is expected to have quadratic computational complexity $O(t_{\text{mem}}^2)$ and was found empirically to scale $\sim 0.95 t_{\text{mem}}^{2.166}$ (where empirical scaling was found based on the data included in the excel file in the [supplementary material](#)). Thus, situations where the reduced dimensionality of the electronic observable of interest leads to longer memory time would increase the computational cost. It should be noted that those observations are consistent with similar observations previously made in Ref. 33, where it was reported that the populations-only GQME gave rise to longer memory times and argued that projecting-out the coherences made it so due to their slower time scale compared to nuclear motion.

To summarize, the scaling of the computational cost with the dimensionality of the electronic observable of interest appears to depend on multiple factors that follow different and sometimes opposing scaling trends. Thus, the computational cost benefits of dimensionality reduction would depend on the balance between those opposing trends, and further work will be needed in order to determine whether or not using a reduced-dimensionality GQME leads to significant saving in computational cost.

V. CONCLUDING REMARKS

The GQME approach provides a general framework for simulating electronic energy, charge, and coherence transfer dynamics, as well as electronic decoherence, in complex molecular systems. Most previous work (with the exception of Refs. 33 and 42) has focused on one specific type of GQME that corresponds to the equation of motion of the full electronic density matrix and can be obtained by projecting-out the nuclear DOF. However, the unfavorable scaling associated with the fact that the memory kernel in this case is N_e^4 -dimensional meant that the range of applicability of this full density matrix GQME was limited to model systems with a relatively small number of electronic states ($N_e \sim 10$).

The reduced-dimensionality GQMEs under consideration in this paper may lead to a more favorable scaling and thereby lower the computational cost. The derivation of those reduced-dimensionality GQMEs is based on the fact that projection superoperators can be chosen that would lead to a GQME for *any* subset of electronic matrix elements in terms of the electronic basis of one's choice. The dimensionality of the memory kernel and inhomogeneous term in such reduced-dimensionality GQMEs reflects the dimensionality of the subset of electronic matrix elements of choice. Since

the PFIs have the same dimensionality as the memory kernel and inhomogeneous term, their calculation, which is typically the computational bottleneck, can be made much more cost effective as a result.

The results reported in this paper for the spin-boson model provide explicit demonstrations of the utility and usefulness of reduced-dimensionality GQMEs. More specifically, we have shown that populations-only, subset, and even scalar single-population GQMEs can improve the accuracy relative to direct application of the input method.

At the same time, it is also important to point out that the scaling of the computational cost with dimensionality depends on other factors as well, some of which appear to follow opposing scaling trends. For example, reduced dimensionality can lead to longer memory times, which would increase the computational cost. Furthermore, reduced dimensionality also can come at the expense of accuracy when approximate input methods are used (although reduced-dimensionality GQMEs are observed to still produce more accurate results than direct application of the input method). Further work will be needed in order to determine the conditions for making reduced-dimensionality GQMEs significantly more cost-effective and finding the optimal balance between reduced dimensionality and accuracy.

Extending the range of applicability of reduced-dimensionality GQMEs to systems with a larger number of electronic states, as well as using a wider variety of inputs methods, both exact and approximate, would be of great interest. Work on such extensions is currently underway and will be reported in future publications.

SUPPLEMENTARY MATERIAL

The [supplementary material](#) includes a pdf with graphs of the PFIs, memory kernels, and inhomogeneous terms for models 2, 4, 5, and 6 along with the imaginary part of the memory kernels of model 1; graphs showing the convergence of the GQME results with the increasing number of trajectories and decreasing time step; and the convergence algorithm used to find the minimum memory time of the GQMEs. The pdf also describes the excel file, also included in the [supplementary material](#), that gives the computational costs of the LSCII dynamics algorithm to obtain the PFIs, the Volterra algorithms for the memory kernels and inhomogeneous terms, and the RK4 algorithm for the GQMEs.

ACKNOWLEDGMENTS

E.G. acknowledges support from the NSF via Grant Nos. 1800325 and 2124511 [CCI Phase I: NSF Center for Quantum Dynamics on Modular Quantum Devices (CQD-MQD)]. The computational resources and services provided by the Advanced Research Computing at the University of Michigan, Ann Arbor, are also acknowledged.

AUTHOR DECLARATIONS

Conflict of Interest

The authors have no conflicts of interest to disclose.

DATA AVAILABILITY

The data that support the findings of this study are available within the article and its [supplementary material](#).

APPENDIX A: DERIVATION OF THE VOLTERRA EQUATIONS OF THE SUBSET QGME FOR ANY COMBINATION OF POPULATIONS AND COHERENCES

In this appendix, we derive the Volterra equations for the memory kernel and inhomogeneous term for the general form of the QGME for any subset of populations and coherences, with the subset of the indices of interest denoted by $\{ab\}$. For the single-population scalar QGME for $\sigma_{jj}(t)$, the subset would be $\{ab\} = \{jj\}$, and for the populations-only QGME, the subset would be $\{ab\} = \{11, 22, \dots, N_e N_e\}$.

We start with the explicit expression for the memory kernel, Eq. (30). We then substitute the following identity for $e^{-i\mathcal{Q}^{\text{sub}}\mathcal{L}\tau/\hbar}$ (the

identity is valid for any projection superoperator \mathcal{Q}):

$$e^{-i\mathcal{Q}\mathcal{L}\tau/\hbar} = e^{-i\mathcal{L}\tau/\hbar} + \frac{i}{\hbar} \int_0^\tau d\tau' e^{-i\mathcal{L}(\tau-\tau')/\hbar} \mathcal{P} \mathcal{L} e^{-i\mathcal{Q}\mathcal{L}\tau'/\hbar}. \quad (\text{A1})$$

This yields the following expression for the matrix elements of $\mathcal{K}^{\text{sub}}(\tau)$:

$$\begin{aligned} \mathcal{K}_{jk,lm}^{\text{sub}}(\tau) &= \frac{1}{\hbar^2} \text{Tr}\left\{(|k\rangle\langle j| \otimes \hat{\mathbf{1}}_n) \mathcal{L} e^{-i\mathcal{L}\tau/\hbar} \mathcal{Q}^{\text{sub}} \mathcal{L} \hat{\rho}_n(0) \otimes |l\rangle\langle m|\right\} \\ &+ \frac{i}{\hbar^3} \int_0^\tau d\tau' \text{Tr}\left\{(|k\rangle\langle j| \otimes \hat{\mathbf{1}}_n) \mathcal{L} e^{-i\mathcal{L}(\tau-\tau')/\hbar} \mathcal{P}^{\text{sub}} \right. \\ &\times \left. \mathcal{L} e^{-i\mathcal{Q}^{\text{sub}}\mathcal{L}\tau'/\hbar} \mathcal{Q}^{\text{sub}} \mathcal{L} \hat{\rho}_n(0) \otimes |l\rangle\langle m|\right\}. \end{aligned}$$

Plugging in $\mathcal{Q}^{\text{sub}} = 1 - \mathcal{P}^{\text{sub}}$ into the first term splits it into two terms. Using \mathcal{P}^{sub} from Eq. (28) in the term that involves \mathcal{P}^{sub} leads to Eq. (32),

$$\begin{aligned} \mathcal{K}_{jk,lm}^{\text{sub}}(\tau) &= \frac{1}{\hbar^2} \text{Tr}\left\{(|k\rangle\langle j| \otimes \hat{\mathbf{1}}_n) \mathcal{L} e^{-i\mathcal{L}\tau/\hbar} \mathcal{L} \hat{\rho}_n(0) \otimes |l\rangle\langle m|\right\} \\ &= \underbrace{i\tilde{F}_{jk,lm}(\tau)} \\ &- \frac{1}{\hbar} \sum_{uv \in \{ab\}} \frac{1}{\hbar} \text{Tr}\left\{(|j\rangle\langle j| \otimes \hat{\mathbf{1}}_n) \mathcal{L} e^{-i\mathcal{L}\tau/\hbar} \hat{\rho}_n(0) \otimes |u\rangle\langle v|\right\} \underbrace{\text{Tr}\left\{(|v\rangle\langle u| \otimes \hat{\mathbf{1}}_n) \mathcal{L} \hat{\rho}_n(0) \otimes |l\rangle\langle m|\right\}}_{=(\mathcal{L}_{uv,lm})_n^0} \\ &+ i \sum_{uv \in \{ab\}} \int_0^\tau d\tau' \frac{1}{\hbar} \text{Tr}\left\{(|k\rangle\langle j| \otimes \hat{\mathbf{1}}_n) \mathcal{L} e^{-i\mathcal{L}(\tau-\tau')/\hbar} \hat{\rho}_n(0) \otimes |u\rangle\langle v|\right\} \frac{1}{\hbar^2} \text{Tr}\left\{(|v\rangle\langle u| \otimes \hat{\mathbf{1}}_n) \mathcal{L} e^{-i\mathcal{Q}^{\text{sub}}\mathcal{L}\tau'/\hbar} \mathcal{Q}^{\text{sub}} \mathcal{L} \hat{\rho}_n(0) \otimes |l\rangle\langle m|\right\}. \\ &= \underbrace{F_{jk,uv}(\tau-\tau')}_{=} \underbrace{K_{uv,lm}^{\text{sub}}(\tau')}_{=} \end{aligned}$$

Note that $(\mathcal{L}_{jj,kk})_n^0 = 0$.

Next, we consider the explicit expression for the inhomogeneous term [Eq. (31)]. We then substitute the identity in Eq. (A1) for $e^{-i\mathcal{Q}^{\text{sub}}\mathcal{L}\tau/\hbar}$, which yields

$$\begin{aligned} I_{jk}^{\text{sub}}(t) &= -\frac{i}{\hbar} \text{Tr}\left\{(|k\rangle\langle j| \otimes \hat{\mathbf{1}}_n) \mathcal{L} e^{-i\mathcal{L}t/\hbar} \left[\hat{\rho}(0) - \sum_{lm \in \{ab\}} \hat{\rho}_n(0) \otimes |l\rangle\langle m| \sigma_{lm}(0) \right]\right\} \\ &+ \frac{1}{\hbar^2} \int_0^t d\tau \text{Tr}\left\{(|k\rangle\langle j| \otimes \hat{\mathbf{1}}_n) \mathcal{L} e^{-i\mathcal{L}(t-\tau)/\hbar} \mathcal{P}^{\text{sub}} \mathcal{L} e^{-i\mathcal{Q}^{\text{sub}}\mathcal{L}\tau/\hbar} \left[\hat{\rho}(0) - \sum_{lm \in \{ab\}} \hat{\rho}_n(0) \otimes |l\rangle\langle m| \sigma_{lm}(0) \right]\right\}. \end{aligned}$$

Splitting the first term into two terms at the minus sign and plugging \mathcal{P}^{sub} from Eq. (28) into the second term lead to Eq. (34),

$$\begin{aligned} I_{jk}^{\text{sub}}(t) &= -\frac{i}{\hbar} \text{Tr}\left\{(|k\rangle\langle j| \otimes \hat{\mathbf{1}}_n) \mathcal{L} e^{-i\mathcal{L}t/\hbar} \hat{\rho}(0)\right\} + i \sum_{lm \in \{ab\}} \frac{1}{\hbar} \text{Tr}\left\{(|k\rangle\langle j| \otimes \hat{\mathbf{1}}_n) \mathcal{L} e^{-i\mathcal{L}t/\hbar} \hat{\rho}_n(0) \otimes |l\rangle\langle m|\right\} \sigma_{lm}(0) \\ &= \underbrace{Z_{jk}^{\text{sub}}(t)}_{=} + \underbrace{F_{jk,lm}(t)}_{=} \\ &+ i \sum_{uv \in \{ab\}} \int_0^t d\tau \frac{1}{\hbar} \text{Tr}\left\{(|k\rangle\langle j| \otimes \hat{\mathbf{1}}_n) \mathcal{L} e^{-i\mathcal{L}(t-\tau)/\hbar} \hat{\rho}_n(0) \otimes |u\rangle\langle v|\right\} \\ &= \underbrace{F_{jk,uv}(t-\tau)}_{=} \\ &\times \left[\underbrace{-\frac{i}{\hbar} \text{Tr}\left\{(|\lambda\rangle\langle \lambda| \otimes \hat{\mathbf{1}}_n) \mathcal{L} e^{-i\mathcal{Q}^{\text{sub}}\mathcal{L}\tau/\hbar} \left[\hat{\rho}(0) - \sum_{lm \in \{ab\}} \hat{\rho}_n(0) \otimes |k\rangle\langle k| \sigma_{kk}(0) \right]\right\}}_{I_{uv}^{\text{sub}}(\tau)} \right]. \end{aligned}$$

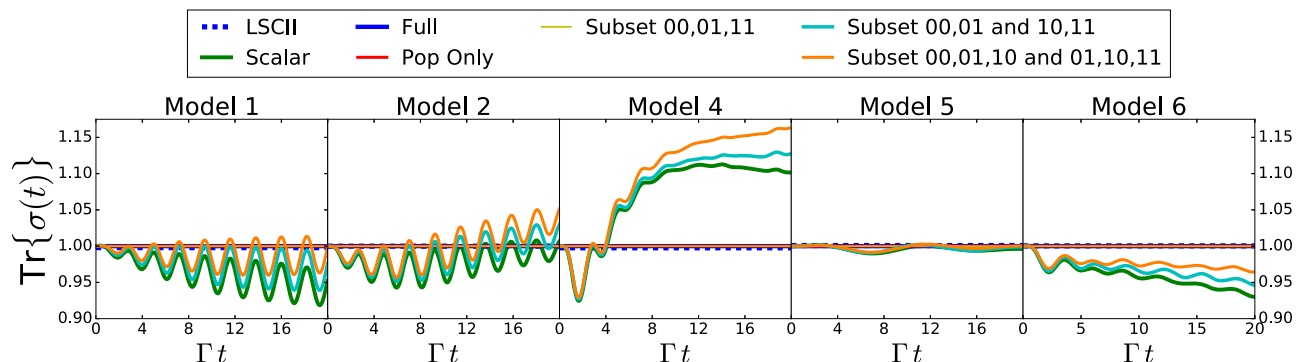


FIG. 10. The trace of the density matrix, $\text{Tr}\{\sigma(t)\} = \sigma_{DD}(t) + \sigma_{AA}(t)$, as a function of time for the five models in Table III. Shown are the results obtained based on the following: direct application of LSCII (dashed blue lines); a combination of the two single-population scalar GQMEs of the form of Eq. (14) for $\sigma_{DD}(t)$ and $\sigma_{AA}(t)$ with LSCII-based PFIs (solid green lines); the full density matrix GQME of the form of Eq. (7) with LSCII-based PFIs (solid blue lines); the populations-only GQME of the form of Eq. (22) with LSCII-based PFIs (solid red lines); a subset GQME of the form of Eq. (29) with $\{ab\} = \{00, 01, 11\}$ with LSCII-based PFIs (solid yellow lines); a combination of two subset GQMEs with $\{ab\} = \{00, 01\}$ and $\{ab\} = \{10, 11\}$ with LSCII-based PFIs (solid cyan lines); and a combination of two subset GQMEs with $\{ab\} = \{00, 01, 10\}$ and $\{ab\} = \{01, 10, 11\}$ with LSCII-based PFIs (solid orange lines).

APPENDIX B: ACCURACY TESTS BASED ON $\text{Tr}\{\hat{\sigma}(t)\} = 1$

Within exact quantum dynamics, the reduced electronic density operator remains normalized at all times such that $\text{Tr}\{\hat{\sigma}(t)\} = \sum_{j=1}^{N_e} \sigma_{jj}(t) = 1$. For a two-state system, this implies that $\sigma_{DD} + \sigma_{AA} = 1$. Since the GQMEs correspond to exact equations of motion, they are also expected to satisfy $\text{Tr}\{\hat{\sigma}(t)\} = 1$ at all times if the memory kernel and inhomogeneous term are obtained from quantum-mechanically exact PFIs. However, this need not be the case when the PFIs are calculated via approximate methods, such as LSCII. In this appendix, we consider the ability of the various GQMEs with LSCII-based PFIs to satisfy $\text{Tr}\{\hat{\sigma}(t)\} = 1$.

The time evolution of $\text{Tr}\{\hat{\sigma}(t)\}$ as obtained from the four types of GQMEs under consideration in this paper with LSCII-based PFIs is shown in Fig. 10. Whereas the full GQME, populations-only GQME, and subset GQME with both populations satisfy $\text{Tr}\{\hat{\sigma}(t)\} = 1$ (see proof below), the scalar single-population GQMEs and subset GQMEs with only one population exhibit significant deviations from it on the population relaxation time scale. This

is consistent with and provides an explanation for our previous observation that single-population scalar GQMEs and subset GQMEs with only a single population underperformed compared to the populations-only, subset with both populations, and full GQMEs.

It can also be shown analytically that any GQME that contains all the populations in its subset of interest (i.e., $\{11, 22, \dots, N_e N_e\} \in \{ab\}$) satisfies $\text{Tr}\{\hat{\sigma}(t)\} = 1$. This includes the full and populations-only GQMEs. Since we know $\text{Tr}\{\hat{\sigma}(0)\} = 1$, the proof is based on showing that its time derivative vanishes. Assuming an initial state $\sigma_{jk}(0) = \delta_{j,k} \sigma_{jj}(0)$ so that $I_{jj}^{\text{sub}}(t) = 0$, the equation of motion for the trace is given by

$$\sum_{j=1}^{N_e} \frac{d}{dt} \hat{\sigma}_{jj}(t) = -\frac{i}{\hbar} \sum_{j=1}^{N_e} \sum_{ik \in \{ab\}} \langle \mathcal{L}_{jj,ik} \rangle_n^0 \hat{\sigma}_{ik}(t) - \sum_{j=1}^{N_e} \sum_{ik \in \{ab\}} \int_0^t d\tau K_{jj,ik}^{\text{sub}}(\tau) \hat{\sigma}_{ik}(t-\tau). \quad (\text{B1})$$

The properties of the Liouvillian give

$$\begin{aligned} \sum_{j=1}^{N_e} \sum_{ik \in \{ab\}} \langle \mathcal{L}_{jj,ik} \rangle_n^0 &= \sum_{j=1}^{N_e} \sum_{ik \in \{ab\}} \delta_{kj} \langle \hat{V}_{ji} \rangle_n^0 - \delta_{ij} \langle \hat{V}_{kj} \rangle_n^0 \\ &= \sum_{j=1}^{N_e} \sum_{ik \in \{ab\}} \delta_{kj} \langle \hat{V}_{ji} \rangle_n^0 - \sum_{j=1}^{N_e} \sum_{ik \in \{ab\}} \delta_{ij} \langle \hat{V}_{kj} \rangle_n^0 \\ &= \sum_{ik \in \{ab\}} \langle \hat{V}_{ki} \rangle_n^0 - \sum_{ik \in \{ab\}} \langle \hat{V}_{ki} \rangle_n^0 = 0. \end{aligned} \quad (\text{B2})$$

So now we just need to prove that the second term, $\sum_{j=1}^{N_e} \sum_{ik \in \{ab\}} \int_0^t d\tau K_{jj,ik}^{\text{sub}}(\tau) \hat{\sigma}_{ik}(t-\tau)$, is also zero. Starting with the memory kernel and summing and expanding over j give

$$\begin{aligned}
 \sum_{j=1}^{N_e} K_{jj,ik}^{\text{sub}}(\tau) &= \sum_{j=1}^{N_e} \frac{1}{\hbar^2} \text{Tr}\{ |j\rangle\langle j| \mathcal{L} e^{-iQ^{\text{sub}} \mathcal{L} \tau / \hbar} Q^{\text{sub}} \mathcal{L} \hat{\rho}_n(0) |i\rangle\langle k| \} = \sum_{j=1}^{N_e} \frac{1}{\hbar^2} \text{Tr}\{ [|j\rangle\langle j|, \hat{H}] e^{-iQ^{\text{sub}} \mathcal{L} \tau / \hbar} Q^{\text{sub}} \mathcal{L} \hat{\rho}_n(0) |i\rangle\langle k| \} \\
 &= \sum_{j=1}^{N_e} \frac{1}{\hbar^2} \text{Tr}\{ (\hat{H}_j - \hat{H}) |j\rangle\langle j| e^{-iQ^{\text{sub}} \mathcal{L} \tau / \hbar} Q^{\text{sub}} \mathcal{L} \hat{\rho}_n(0) |i\rangle\langle k| \} \\
 &\quad + \sum_{\substack{j,l=1 \\ l \neq j}}^{N_e} \frac{1}{\hbar^2} \text{Tr}\{ \hat{V}_{jl} |j\rangle\langle l| e^{-iQ^{\text{sub}} \mathcal{L} \tau / \hbar} Q^{\text{sub}} \mathcal{L} \hat{\rho}_n(0) |i\rangle\langle k| \} - \sum_{\substack{j,l=1 \\ l \neq j}}^{N_e} \frac{1}{\hbar^2} \text{Tr}\{ \hat{V}_{lj} |l\rangle\langle j| e^{-iQ^{\text{sub}} \mathcal{L} \tau / \hbar} Q^{\text{sub}} \mathcal{L} \hat{\rho}_n(0) |i\rangle\langle k| \} \\
 &= \sum_{\substack{j,l=1 \\ l \neq j}}^{N_e} \frac{1}{\hbar^2} \text{Tr}\{ \hat{V}_{jl} |j\rangle\langle l| e^{-iQ^{\text{sub}} \mathcal{L} \tau / \hbar} Q^{\text{sub}} \mathcal{L} \hat{\rho}_n(0) |i\rangle\langle k| \} - \sum_{\substack{j,l=1 \\ l \neq j}}^{N_e} \frac{1}{\hbar^2} \text{Tr}\{ \hat{V}_{jl} |j\rangle\langle l| e^{-iQ^{\text{sub}} \mathcal{L} \tau / \hbar} Q^{\text{sub}} \mathcal{L} \hat{\rho}_n(0) |i\rangle\langle k| \} \\
 &= 0.
 \end{aligned} \tag{B3}$$

Plugging the results of Eqs. (B2) and (B3) into Eq. (B1) shows that the equation of motion for the trace is zero, $\sum_{j=1}^{N_e} \frac{d}{dt} \sigma_{jj}(t) = 0$, and therefore, the trace will remain at 1.

The ability of the various GQMEs with LSCII-based PFIs to satisfy $\text{Tr}\{\hat{\sigma}(t)\} = 1$ can also be elucidated from another perspective

by considering the following three ways for calculating $\sigma_z(t)$, which should give the same result if $\text{Tr}\{\hat{\sigma}(t)\} = 1$:

1. $\sigma_z(t) = \sigma_{DD}(t) - \sigma_{AA}(t)$,
2. $\sigma_z(t) = 2\sigma_{DD}(t) - 1$, and
3. $\sigma_z(t) = 1 - 2\sigma_{AA}(t)$.

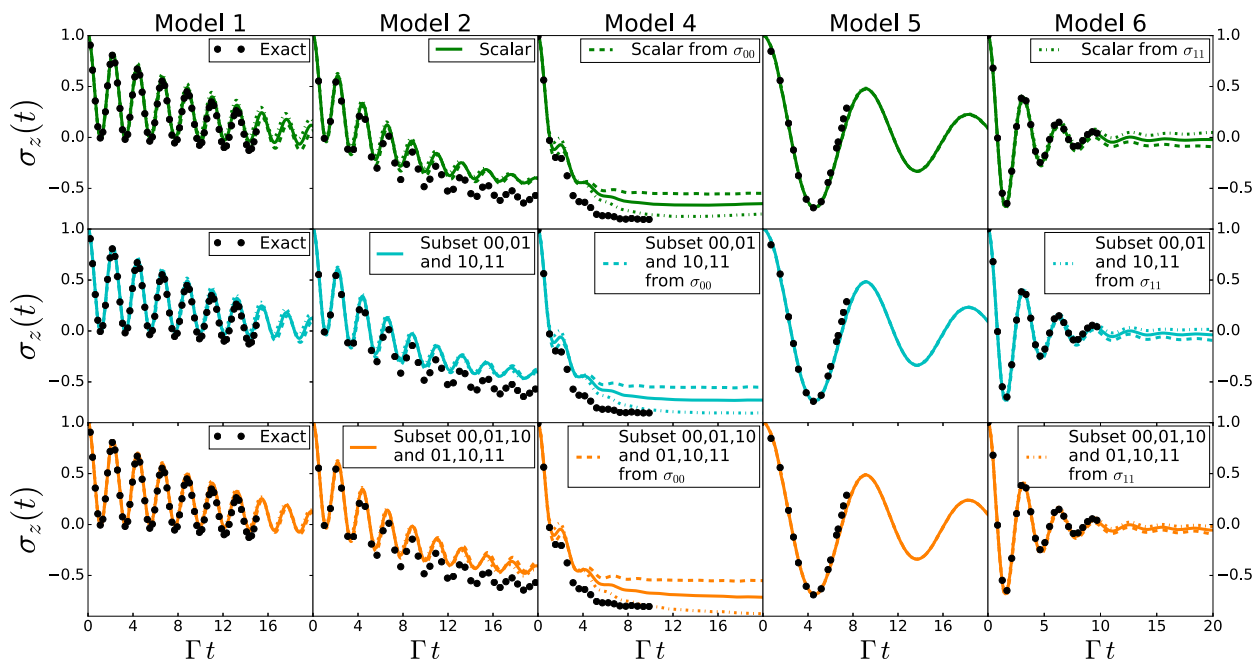


FIG. 11. Electronic population difference, $\sigma_z(t)$, as a function of time for the five models in Table III. In the first row, shown are exact results (black circles) and results obtained based on single-population scalar GQMEs of the form of Eq. (14) calculated in three ways: (1) $\sigma_z(t) = \sigma_{DD}(t) - \sigma_{AA}(t)$ with LSCII-based PFIs (solid green lines), (2) $\sigma_z(t) = 2\sigma_{DD}(t) - 1$ with LSCII-based PFIs (dashed green lines), and (3) $\sigma_z(t) = 1 - 2\sigma_{AA}(t)$ with LSCII-based PFIs (dashed-dotted green lines). In the second row, shown are exact results (black circles) and results obtained based on a subset GQME of the form of Eq. (29) where $\{ab\} = \{00, 01\}$ for the $\sigma_{00}(t)$ dynamics and $\{ab\} = \{10, 11\}$ for the $\sigma_{11}(t)$ dynamics. This subset GQME can be calculated in three ways: (1) $\sigma_z(t) = \sigma_{DD}(t) - \sigma_{AA}(t)$ with LSCII-based PFIs (solid cyan lines), (2) $\sigma_z(t) = 2\sigma_{DD}(t) - 1$ with LSCII-based PFIs (dashed cyan lines), and (3) $\sigma_z(t) = 1 - 2\sigma_{AA}(t)$ with LSCII-based PFIs (dashed-dotted cyan lines). In the third row, shown are exact results (black circles) and results obtained based on a subset GQME of the form of Eq. (29) where $\{ab\} = \{00, 01, 10\}$ for the $\sigma_{00}(t)$ dynamics and $\{ab\} = \{01, 10, 11\}$ for the $\sigma_{11}(t)$ dynamics. This subset GQME can be calculated in three ways: (1) $\sigma_z(t) = \sigma_{DD}(t) - \sigma_{AA}(t)$ with LSCII-based PFIs (solid orange lines), (2) $\sigma_z(t) = 2\sigma_{DD}(t) - 1$ with LSCII-based PFIs (dashed orange lines), and (3) $\sigma_z(t) = 1 - 2\sigma_{AA}(t)$ with LSCII-based PFIs (dashed-dotted orange lines).

Indeed, we verified that those three ways of calculating $\sigma_z(t)$ yield the same results in the case of the populations-only and full GQMEs and the subset with both populations. However, this is not the case for the single-population scalar GQMEs and subset GQMEs with only one of the populations, where there are significant differences between the results obtained via the three ways (see Fig. 11). Calculating $\sigma_z(t)$ the first way appears to give the best results with the exception of model 4, where calculating it the third way gives the best results.

REFERENCES

- ¹D. Xu and K. Schulten, *Chem. Phys.* **182**, 91 (1994).
- ²A. Ishizaki and G. R. Fleming, *Annu. Rev. Condens. Matter Phys.* **3**, 333 (2012).
- ³P. A. Liddell, D. Kuciauskas, J. P. Sumida, B. Nash, D. Nguyen, A. L. Moore, T. A. Moore, and D. Gust, *J. Am. Chem. Soc.* **119**, 1400 (1997).
- ⁴P. A. Liddell, G. Kodis, A. L. Moore, T. A. Moore, and D. Gust, *J. Am. Chem. Soc.* **124**, 7668 (2002).
- ⁵J.-L. Brédas, D. Beljonne, V. Coropceanu, and J. Cornil, *Chem. Rev.* **104**, 4971 (2004).
- ⁶A. C. Rizzi, M. van Gastel, P. A. Liddell, R. E. Palacios, G. F. Moore, G. Kodis, A. L. Moore, T. A. Moore, D. Gust, and S. E. Braslavsky, *J. Phys. Chem. A* **112**, 4215 (2008).
- ⁷H. Tian, Z. Yu, A. Hagfeldt, L. Kloo, and L. Sun, *J. Am. Chem. Soc.* **133**, 9413 (2011).
- ⁸A. Mishra, M. K. R. Fischer, and P. Bäuerle, *Angew. Chem., Int. Ed.* **48**, 2474 (2009).
- ⁹S. M. Feldt, E. A. Gibson, E. Gabrielsson, L. Sun, G. Boschloo, and A. Hagfeldt, *J. Am. Chem. Soc.* **132**, 16714 (2010).
- ¹⁰Y. Zhao and W. Liang, *Chem. Soc. Rev.* **41**, 1075 (2012).
- ¹¹M. H. Lee, B. D. Dunietz, and E. Geva, *J. Phys. Chem. C* **117**, 23391 (2013).
- ¹²M. H. Lee, B. D. Dunietz, and E. Geva, *J. Phys. Chem. Lett.* **5**, 3810 (2014).
- ¹³H.-D. Meyer, F. Gatti, and G. A. Worth, *Multidimensional Quantum Dynamics: MCTDH Theory and Applications* (John Wiley & Sons, 2009).
- ¹⁴N. Makri, *Annu. Rev. Phys. Chem.* **50**, 167 (1999).
- ¹⁵J. Jin, X. Zheng, and Y. Yan, *J. Chem. Phys.* **128**, 234703 (2008).
- ¹⁶Y. Tanimura and R. Kubo, *J. Phys. Soc. Jpn.* **58**, 101 (1989).
- ¹⁷Y. Tanimura, *Phys. Rev. A* **41**, 6676 (1990).
- ¹⁸Y. Tanimura, *J. Phys. Soc. Jpn.* **75**, 082001 (2006).
- ¹⁹S. M. Greene and V. S. Batista, *J. Chem. Theory Comput.* **13**, 4034 (2017).
- ²⁰S. Nakajima, *Prog. Theor. Phys.* **20**, 948 (1958).
- ²¹R. Zwanzig, *J. Chem. Phys.* **33**, 1338 (1960).
- ²²Q. Shi and E. Geva, *J. Chem. Phys.* **119**, 12063 (2003).
- ²³Q. Shi and E. Geva, *J. Chem. Phys.* **120**, 10647 (2004).
- ²⁴M.-L. Zhang, B. J. Ka, and E. Geva, *J. Chem. Phys.* **125**, 044106 (2006).
- ²⁵B. J. Ka, M.-L. Zhang, and E. Geva, *J. Chem. Phys.* **125**, 124509 (2006).
- ²⁶G. Cohen and E. Rabani, *Phys. Rev. B* **84**, 075150 (2011).
- ²⁷E. Y. Wilner, H. Wang, G. Cohen, M. Thoss, and E. Rabani, *Phys. Rev. B* **88**, 045137 (2013).
- ²⁸G. Cohen, E. Y. Wilner, and E. Rabani, *New J. Phys.* **15**, 073018 (2013).
- ²⁹G. Cohen, E. Gull, D. R. Reichman, A. J. Millis, and E. Rabani, *Phys. Rev. B* **87**, 195108 (2013).
- ³⁰A. Kelly and T. E. Markland, *J. Chem. Phys.* **139**, 014104 (2013).
- ³¹L. Kidon, E. Y. Wilner, and E. Rabani, *J. Chem. Phys.* **143**, 234110 (2015).
- ³²W. C. Pfalzgraff, A. Kelly, and T. E. Markland, *J. Phys. Chem. Lett.* **6**, 4743 (2015).
- ³³A. Montoya-Castillo and D. R. Reichman, *J. Chem. Phys.* **144**, 184104 (2016).
- ³⁴A. Kelly, N. Brackbill, and T. E. Markland, *J. Chem. Phys.* **142**, 094110 (2015).
- ³⁵A. Kelly, A. Montoya-Castillo, L. Wang, and T. E. Markland, *J. Chem. Phys.* **144**, 184105 (2016).
- ³⁶L. Kidon, H. Wang, M. Thoss, and E. Rabani, *J. Chem. Phys.* **149**, 104105 (2018).
- ³⁷W. C. Pfalzgraff, A. Montoya-Castillo, A. Kelly, and T. E. Markland, *J. Chem. Phys.* **150**, 244109 (2019).
- ³⁸E. Mulvihill, A. Schubert, X. Sun, B. D. Dunietz, and E. Geva, *J. Chem. Phys.* **150**, 034101 (2019).
- ³⁹E. Mulvihill, X. Gao, Y. Liu, A. Schubert, B. D. Dunietz, and E. Geva, *J. Chem. Phys.* **151**, 074103 (2019).
- ⁴⁰E. Mulvihill, K. M. Lenn, X. Gao, A. Schubert, B. D. Dunietz, and E. Geva, *J. Chem. Phys.* **154**, 204109 (2021).
- ⁴¹E. Mulvihill and E. Geva, *J. Phys. Chem. B* **125**, 9834 (2021).
- ⁴²N. Ng, D. T. Limmer, and E. Rabani, *J. Chem. Phys.* **155**, 156101 (2021).
- ⁴³R. Zwanzig, *Nonequilibrium Statistical Mechanics* (Oxford University Press, New York, 2001).
- ⁴⁴A. Nitzan, *Chemical Dynamics in Condensed Phases* (Oxford University Press, New York, 2006).
- ⁴⁵S. Mukamel, *Principles of Nonlinear Optical Spectroscopy* (Oxford University Press, New York, 1995).
- ⁴⁶H.-P. Breuer and F. Petruccione, *The Theory of Open Quantum Systems* (Oxford University Press, New York, 2002).
- ⁴⁷X. Sun, H. Wang, and W. H. Miller, *J. Chem. Phys.* **109**, 4190 (1998).
- ⁴⁸K. Thompson and N. Makri, *J. Chem. Phys.* **110**, 1343 (1999).